# In-beam $\gamma$-ray spectroscopy of low- and medium-spin levels in $^{211}$Po

J. M. K. Slotte,[1,*] P. Granholm,[1,2] R. Öhman,[1] T. Lönnroth,[1] S. Juutinen,[3] J. Suhonen,[3] P. M. Jones,[3,4] R. Julin,[3] J. Pakarinen,[3] P. Rahkila,[3] C. Scholey,[3] J. Sorri,[3] and J. Uusitalo[3]

[1]*Physics, Faculty of Science and Engineering, Åbo Akademi University, Turku FIN-20500, Finland*

[2]*Faculty of Business, ICT and Chemical Engineering, Turku University of Applied Sciences, Turku FIN-20520, Finland*

[3]*Department of Physics, University of Jyväskylä, Jyväskylä FIN-40014, Finland*

[4]*iThemba LABS, National Research Foundation, P.O. Box 722, Somerset West 7129, South Africa*

(Received 29 January 2017; published 3 October 2017)

The structure of the low- and medium-spin levels of the $^{211}$Po nucleus have been studied with in-beam $\gamma$-ray spectroscopy with the $^{208}$Pb$(\alpha,n)^{211}$Po fusion-evaporation reaction. The level scheme was further extended with levels of the configurations $\pi(h_{9/2})^2_{2^+-4^+}\otimes\nu g_{9/2}$, $\pi(h_{9/2})^2_{8^+}\otimes\nu g_{9/2}$, $\pi(h_{9/2})^2_{2^+-4^+}\otimes\nu i_{11/2}$, $\pi(h_{9/2})^2_{2^+-4^+}\otimes\nu j_{15/2}$, $\pi(h_{9/2}f_{7/2})_{8^+}\otimes\nu g_{9/2}$, and $\pi(h_{9/2})^2_{0^+}\otimes\nu(g_{9/2})^2_{0^+}(s_{1/2})^{-1}$. The single-particle neutron states $\nu d_{5/2}$ and $\nu s_{1/2}$ were also identified. Furthermore, a number of states feeding the low-spin structures were added.

DOI: 10.1103/PhysRevC.96.044302

## I. INTRODUCTION

### A. The nuclide $^{211}$Po

One of the more successful models in describing the structures of nuclei is the shell model, where the structure of a nucleus is built from individual nucleons coupled together to create a greater whole. The interaction between the valence nucleons determine, for the most part, the properties of the levels in a nucleus while the other nucleons often form an inert core. And now with the advent, during the past decade, of more realistic shell-model calculations [1] and the improved roles of genuine and effective three-body forces for heavy nuclei, the prospects of future explorations seem promising. The best available testing ground for shell-model calculations in the heavy-element region is near the doubly magic $^{208}$Pb nucleus. It is therefore important to have as a complete picture as possible of these nuclei. Even with a wide variety of experiments covering the $^{208}$Pb region, performed over a long time span, there still remains nuclei with experimental gaps. This is mostly due to the difficulties of producing the nuclei in the $^{208}$Pb region with stable-ion beams.

One such experimental gap is the nucleus $^{211}$Po with mainly yrast and high-spin levels identified. With two protons and one neutron above their corresponding closed shells ($Z = 82$ and $N = 126$), the $^{211}$Po nucleus is an interesting specimen to study not only from a shell-model perspective but also as a general test bed for other models with three-particle interactions. The shells $1g_{9/2}$, $0i_{11/2}$, and $0j_{15/2}$ are considered to be the main actors on the neutron side, while the shells $0h_{9/2}$, $1f_{7/2}$, and $0i_{13/2}$ play a similar part on the proton side. The isotope $^{211}$Po is also one of the classic examples of yrast spin-gap isomers [2] of nuclei with its isomeric state of $25/2^+$ at 1462 keV, adding another hurdle for models to take into account.

### B. Review of previous works

The first shell-model calculations on $^{211}$Po were preformed by Auerbach and Talmi in an attempt to describe the $25/2^+$ isomeric state [3] in the same way that they were able to successfully describe the isomeric state of $^{93}$Mo. The interaction matrices were written in the form $|h^2_{9/2}(J_1)g_{9/2}J\rangle$ with the $\pi h_{9/2}\nu g_{9/2}$ interaction taken from $^{210}$Bi and the $h^2_{9/2}$ interaction taken from $^{210}$Po. The calculated $J = 25/2$ level was 1.46 MeV above the ground state compared to, at that time, known experimental value of 1.45 MeV for the isomeric state. The spin gap in $^{211}$Po was shown to arise due to the attraction between a $h_{9/2}$ proton and a $g_{9/2}$ neutron, which is stronger in the highest spin state $J = 9$, than in the states $J = 8$–4. Accordingly, all the calculated 23/2, 21/2, and 19/2 levels were shown to be above the 25/2 state.

Faestermann *et al.* obtained a mean life of $\tau = 23 \pm 2$ ns and a $g$ factor of $-0.05 \pm 0.02$ for the 1065-keV $15/2^-$ state by using a pulsed $\alpha$-particle beam of 22.5 MeV on $^{208}$Pb [4]. The measured lifetime and positive $A_2$ were consistent with an enhanced $E3$ transition of 18 W.u. between the $15/2^-$ and $9/2^+$ states.

By studying the protons from the one-neutron stripping reaction $^{210}$Po$(d,p)^{211}$Po at 17 MeV, 35 levels were observed by Bhatia *et al.* up to 3.9 MeV excitation [5]. Extraction of spectroscopic factors and $l$-value assignments for many levels were made possible by comparing experimental angular distributions with distorted-wave Born approximation (DWBA) calculations. It was also shown that a simple particle-vibration coupling model was inadequate to describe the observed level structure in $^{211}$Po. In terms of binding energy, it was seen that the low-lying states are more bound in $^{211}$Po than in $^{209}$Pb. It was indicated that the particle-core interaction is increased for low-lying states and less effective for states higher up in energy.

By using a basis that contains correlated particle pairs, Silvestre-Brac and Boisson preformed exact shell-model calculations for nuclei consisting of three nonidentical particles outside of the $^{208}$Pb core [6]. The Kuo-Herling (KH) and Kim-Rasmussen (KR) interactions were tested and compared to earlier experimental data. Even though some levels differed by some 300 keV, the level scheme was roughly the same with both interactions. The KR energies were slightly better

*joakim.slotte@abo.fi

 

while KH had better spectroscopic factors (neutrons on the $0^+$ ground state on $^{210}$Po). An yrast trap of $31/2^-$ at around 2.4 MeV and a $37/2^+$ isomeric state at 3.5 MeV were predicted by both the KH and KR interactions.

Fant *et al.* studied the excited states of $^{211}$Po through the reaction $^{208}$Pb($\alpha$,$n$), in the $\alpha$-particle energy ranges of 18.0–20.6 MeV by means of in-beam $\gamma$-ray and conversion-electron spectroscopy [7]. Spins and parities were determined, via angular distributions and electron conversions, for several states with the yrast spin values ranging from 1/2 to 17/2 and 25/2. Three isomeric states were observed, the $15/2^-$ at 1064.8 keV, the $1/2^-$ at 1578 keV, and the (21/2) state at around 1500 keV with their respective half-lives of 14(1), 3.5(3), and 20(5) ns. Levels were mostly explained by coupling the two $h_{9/2}$ protons to total spin of $0^+$, $2^+$, and $4^+$ to which the odd $g_{9/2}$ neutron is thereafter coupled. Excitation of the neutron to $i_{11/2}$ and $j_{15/2}$ was also observed. A corresponding neutron hole excitation $[\pi(h_{9/2})^2_0 \otimes \nu(g_{9/2})^2(p_{1/2})^{-1}]_{1/2^-}$ at 1578 keV was discussed briefly.

Warburton [8] performed shell-model calculations for $^{211}$Po using a modified Kuo-Herling nucleon-nucleon interaction, and the results agreed fairly well with the measurements done by Bhatia [5] and Fant [7]. An yrast spectrum was presented for comparison to anticipated results from fusion-evaporation reaction studies. The experimental $^{210}$Po$(d,p)^{211}$Po spectroscopic factors were rather accurately reproduced.

Discussions of how much of the feeding from high-lying high-spin states will bypass the $25/2^+$ isomer and therefore be seen in coincidence with $\gamma$-ray transitions between the low-lying states were also held. Warburton predicted the $21/2^+$, $19/2^+$, and $23/2^+$ yrast states at 1505, 1546, and 1646 keV, and the decays of these states can be expected, at least partially, to bypass the $25/2^+$ isomer.

High-spin states in $^{211}$Po were later studied by McGoram *et al.* [9], in a series of measurements through the incomplete fusion and/or breakup reactions $^{208}$Pb($^9$Be,$\alpha 2n$) and $^{208}$Pb($^7$Li,$p3n$) with different experimental conditions. As a result of this study, the yrast structure was extended up to $J^\pi = (43/2)^+$ at 4873 keV, and further, two isomers were identified with lifetimes of 350(30) ns and 4(1) $\mu$s at the excitation energies of 2136 keV ($31/2^-$) and 4873 keV ($43/2^+$), respectively. The measured lifetime of the (21/2) isomer, now mentioned as 1428+$\Delta$ keV, was 36(2) ns. To structurally describe the higher spin states, the following proton configurations were used: $\pi(h_{9/2})^2_{8^+}$, $\pi(h_{9/2}i_{13/2})$, $\pi(h_{9/2}f_{7/2})$ coupled with neutrons in the $g_{9/2}$, $i_{11/2}$, $j_{13/2}$, $(g^2_{9/2}p^{-1}_{1/2})$, $(g_{9/2}i_{11/2}p^{-1}_{1/2})$, $(g^2_{9/2}f^{-1}_{5/2})$, and $(i_{11/2}j_{15/2}p^{-1}_{1/2})$ states.

Empirical multiparticle shell-model calculations were also performed for $^{211}$Po, by McGoram *et al.* [9], with the active proton orbitals being the $0h_{9/2}$, $1f_{7/2}$, and $0i_{13/2}$, and the active neutron orbitals being the $1g_{9/2}$, $0i_{11/2}$ and $0j_{15/2}$, including excitations across the $N = 126$ neutron shell gap of which the $\nu g_{9/2}p^{-1}_{1/2}$ particle-hole pair was likely to be least energy expensive. The results of these calculations agreed well with the experimental values. The high-level density above the 1428+$\Delta$ keV (21/2) isomer, i.e., at energies of 1428–2500 keV, also needed mentioning. The likely origin of these levels are seniority 3 states of the following configurations: $\pi(h_{9/2})^2_J \otimes \nu(g_{9/2})$, $\pi(h_{9/2})^2_J \otimes \nu(i_{11/2})$, $\pi(h_{9/2}f_{7/2})_J \otimes \nu(g_{9/2})$, and $\pi(h_{9/2}f_{7/2})_J \otimes \nu(i_{11/2})$.

Using the deep inelastic collisions, with $^{76}$Ge at 450 MeV on $^{208}$Pb, with the goal to populate nuclei in the vicinity of $^{208}$Pb, Fornal *et al.* also studied the high-spin states above the $25/2^+$ $\alpha$-decaying isomer in $^{211}$Po [10]. The same isomers as in Ref. [9] were detected with measured lifetime of 0.25(7) $\mu$s for the ($31/2^-$) state and 2(1) $\mu$s for the ($43/2^+$) state. In their interpretation of the ($37/2^-$) and the ($43/2^+$) states, Fornal *et al.* characterized both isomers as part of a core $^{208}$Pb excitation, in the form of $(\pi h^2_{9/2} \otimes \nu i_{11/2})_{27/2^+} \otimes 5^-$ and $(\pi h_{9/2}i_{13/2} \otimes \nu i_{11/2})_{33/2^+} \otimes 5^-$ respectively whereas McGoram *et al.* [9] assigned the configurations $\pi(h^2_{9/2}) \otimes \nu(g_{9/2}i_{11/2}p^{-1}_{1/2})$ for the $37/2^-$ state and $\pi(h_{9/2}i_{13/2}) \otimes \nu(g_{9/2}i_{11/2}p^{-1}_{1/2})$ for the $43/2^+$ state.

Single-particle states in the doubly magic $^{132}$Sn region have corresponding single-particle states around $^{208}$Pb with one unit larger angular momenta $l$ and $j$. Fornal *et al.* compared the yrast level structures of the three-valence-particle nucleus $^{135}$Te with $^{211}$Po [11]. The ordering of the corresponding states was the same and their relative energy spacings were similar, and therefore it was concluded that more complex shell-model configurations were also similar between the different regions of doubly magic nuclei.

Sun and Guo investigated the possibility of neutron halos in the excited states for $N = 127$ isotones using a nonlinear relativistic mean-field theory [12]. The results of the calculations agreed with the experimental data of neutron halos in the excited states of $^{209}$Pb. Furthermore, neutron halos were predicted to exist in the excited states of $2d_{5/2}$, $3s_{1/2}$, and $2d_{3/2}$ in $^{207}$Hg, $^{208}$Tl, $^{210}$Bi, and finally in $^{211}$Po.

### C. Aim of the present work

The main aim of the present work was to characterize the non-yrast low- and medium-spin states and thereby complement the structural studies by Fant *et al.* and McGoram *et al.* [7,9]. The reaction mechanism was chosen to be the same as in Ref. [7] but with a slightly higher energy, and the details of the present experimental setup are briefly discussed in Sec. II. The results and level schemes are presented in Sec. III. The configurations of the different levels are discussed in Sec. IV and finally a summary is given in Sec. V.

## II. EXPERIMENT AND DATA ANALYSIS

The reaction $^{208}$Pb($\alpha$,$n$) was used to populate excited states in $^{211}$Po. An enriched $^{208}$Pb 8–10mg/cm$^2$ target foil was bombarded by a 23-MeV $\alpha$-particle beam, with an average beam current of 13 particle nA, provided by the K130 cyclotron at the Accelerator Laboratory at the Department of Physics of the University of Jyväskylä (JYFL), Finland. Utilizing the JUROGAM I array with 43 compton-suppressed HPGe detectors, the prompt $\gamma$ rays were detected. The detectors were installed in six rings around the target chamber with the angles 72.05°, 85.84°, 94.16°, 107.94°, 133.57°, and 157.60° with respect to the beam direction. The energy resolution for HPGe detectors were 2.5 keV at 1332 keV. A total of $1.1 \times 10^7$

singles events were collected during 8 h of beam time. The triggerless Total Data Readout (TDR) acquisition system [13] was used to time stamp the events. Data were sorted offline with GRAIN [14] and analyzed with the RADWARE software packages [15,16].

Where feasible, $\gamma$-ray angular distributions were determined for the more intense transitions. The intensities, determined from spectra of the individual detector rings, were fitted to Legendre polynomials of the form $W(\theta) = A_0 + A_2P_2(\cos\theta) + A_4P_4(\cos\theta)$ [17]. In cases where the angular distribution fits yielded lower $\chi^2$ values when $A_4$ was left out, they are presented as such. To complement the angular distribution analysis, a form of angular anisotropies were also used. In our case, the anisotropy is defined as $A = \frac{W(72.5^\circ)+W(157.60^\circ)}{2W(94.16^\circ)}$ and was especially useful when statistics were too poor to fit the normal angular distribution. After detector efficiency corrections, some typical values for the anisotropies for pure stretched transitions were 0.76–0.98 for quadrupole transitions and 0.54–0.81 for dipole transitions. Pure transitions of the type $\Delta J = 0$ were between 0.37 and 0.46 for quadrupole transitions and between 1.15 and 1.26 for dipole transitions, while nonstretched $\Delta J = 1$ quadrupole transitions have their values between 1.34 and 2.29 for downward and between 0.61 and 0.88 for upward transitions.

Another way to determine the multipole of transitions is by $\gamma$-ray angular distribution from oriented nuclei (ADO) ratios [18]. The main advantage with the ADO ratio is that it is independent of the gating transition. Experimentally the ADO can be seen, in our case, as $\mathrm{I}(\gamma_1 : 90^\circ, \gamma_2\text{:all})/I(\gamma_1 : 133^\circ, \gamma_2\text{:all})$. Here $I(\gamma_1\text{:}\theta, \gamma_2\text{:all})$ is the intensity of the observed $\gamma$ ray at the angle $\theta$ by setting gates on detectors to allow for any angle. This method requires the construction of two $\gamma$-$\gamma$ matrices, corresponding to $\theta_1$ vs all and $\theta_2$ vs all. In the case of sorting $\gamma$-$\gamma$ matrices for the ADO analysis, the detector rings at 85.84° and 94.16° were combined to form a new ring at 90°. Typical ADO values in this experiment were 0.6 for stretched pure dipole transitions and 1.0 for stretched pure quadrupole transitions. Some care must be taken as the ADO ratios cannot differentiate between $\Delta J = 0$ dipoles or certain $\Delta J = 1$ mixed transitions and stretched $E2$s. New transitions and previously unassigned transitions were assigned $E2$ multipolarity for stretched quadrupole transitions and pure dipole transitions were assigned $M1$ or $E1$ multipolarity. Mixed transitions are assumed to be of the $E2/M1$ type.

## III. RESULTS AND LEVEL SCHEME

The properties of the $\gamma$ rays originating from $^{211}$Po are summarized in Table I. New transitions have their energies marked with a $^{\mathrm{n}}$, e.g., 138.73(4)$^{\mathrm{n}}$.

Most $\gamma$-ray intensities are taken from coincidence spectra and in the cases where the intensity is determined from the single spectrum the intensity is noted with an asterisk (*) after it. Only in cases where the both the spin and parity are known of levels involved in a transition is the multipolarity explicitly written. In general, the statistical data gathered in the current work is improved compared to Ref. [7] and the differences in the intensities of earlier known transitions depend, with the higher energy of the incoming $\alpha$ particle in the reaction, on the feeding of levels higher in energy and spin.

The total projection spectrum of the $E_\gamma$-$E_\gamma$ matrix is shown in Fig. 1. Two dominating peaks in Fig. 1, the 245-keV and partly the 1181-keV peaks, have their origin in $^{210}$Po. The strong presence of $^{210}$Po, with levels identified up to the $7^+$ state at 2438-keV level, compared to Ref. [7] was to be expected as the beam energy of 23 MeV is well above the $(\alpha,2n)$ threshold and the cross section for the $(\alpha,n)$ channel is rather small at this energy [19].

With higher beam energy, the higher spin states in $^{211}$Po were more emphasized, as can be seen, for example, by the less prominent 193-keV transition and the overall increased intensity along the yrast cascade compared to Ref. [7].

Of some interest are the unidentified peaks at 709, 1264, and 1274 keV, which are also found in Ref. [7]. The 709- and 1264-keV peaks are marked in Fig. 1 and the 1274-keV peak is after 1264 keV. Of these peaks, the 1274-keV one is also seen in the background spectra. No feasible background radiation correspond to these energies, and neither does gating on these energies and their coincident events help to place these $\gamma$-ray transitions in current known level schemes.

### A. Construction of level schemes

The level scheme of $^{211}$Po has been built and expanded in accordance with the findings of current work. The level scheme is presented as partial level schemes (see Figs. 2–5) and highlights cascades through different levels. A selection of gates obtained from the $E_\gamma$-$E_\gamma$ matrix are shown in the Figs. 6 and 7. A few peaks in Fig. 6 and certain areas in Fig. 7 have been rescaled. In both cases, scaling factors are placed next to the peaks in question or in the relevant parts of the spectrum. Where larger intensities of chance coincidences or contaminants make an appearance, these are marked with asterisks.

In Fig. 6(a), the gated spectrum of the 363-keV $\gamma$ transition is shown while the partial level scheme in Fig. 2 mainly shows the levels above the $17/2^+$ level at 1427 keV. In current work, a gating time of 100 ns was used and thus transitions to the $1427 + \Delta$ keV level, with a lifetime of 36(2) ns [9], could be measured. Distinguishing between transitions cascading via the $1427 + \Delta$ keV level and other transitions coming directly to the $17/2^+$ level at 1427 keV is hard. Therefore, new $\gamma$ transitions feeding the $17/2^+$ level at 1427 keV, but not in coincidence with previously known transition originating from levels above 1427 keV, are placed above this level, while technically they could decay via the $(21/2^+)$ isomer at $1427 + \Delta$ keV.

The $\gamma$-ray transitions 152 and 425 keV are seen in coincidence with the 188-keV transition and have been moved from their previous placings [9], i.e., between 1616 and 1427 keV and between 1853 and 1427 keV, respectively. The new initial levels are 1768 keV for the 152-keV transition and 2041 keV for the 425-keV transition. The new $\gamma$-ray transition of 538 keV coincides with both the 188- and 425-keV transitions. Using intensity arguments, the 538-keV $\gamma$-ray transition is placed to originate from a new level at

TABLE I. The first three columns give energies of the $\gamma$ ray and of the initial and final states involved in the decay. Transitions marked with [n] are not reported earlier. The fourth column gives the $\gamma$-ray intensities normalized to the 1064-keV transition. Intensities taken from the single spectrum are marked with [s], whereas the rest are taken from coincidence spectrum. Columns 5, 6, and 7 show the results of the anisotropy, angular distribution, and ADO "fits." The last columns supply the assigned multipolarities of the transition and the spins of the involved states. Mixing ratios were not deduced and transitions assigned as having a multipolarity of dipoles may include some quadrupole admixture. Quoted errors are statistical only. The gated transition used to acquire the ADO values are marked in the following way: a, 193 keV; b, 278 keV; c, 335 keV; d, 363 keV; e, 392 keV; f, 687 keV; g, 796 keV; h, 1028 keV; i, 1050 keV; j, 1121 keV; k, 1161 keV; l, 1181 keV; m, 687+363 keV.

| $\gamma$-ray energy $E_\gamma$ (keV) | Initial state $E_i$ (keV) | Final state $E_f$ (keV) | Intensity $I_\gamma$ | Anisotropy $A$ | Angular $A_2/A_0$ | distribution $A_4/A_0$ | ADO | Multi-polarity | $I_i^\pi$ | $I_f^\pi$ |
|---|---|---|---|---|---|---|---|---|---|---|
| 113.27(3) | 1540.7(3) | 1427.4(2) | 1.43(5) | 1.7(5) | 0.12(4) | −0.30(9) | 0.97[d] | $q$ | (21/2) | $17/2^+$ |
| 138.73(4)[n] | 1597.7(8) | 1458.7(2) | 0.45(2) | 0.9(2) | −0.12(4) | 0.28(8) | | $q$ | 13/2 | 15/2 |
| 152.10(4) | 1767.8(4) | 1615.7(3) | 0.25(1) | | | | | | | |
| 165.62(6)[n] | 1682.6(4) | 1517.0(2) | 0.18(1) | | | | | | (7/2,9/2,11/2) | (7/2,9/2,11/2) |
| 168.47(5) | 1904.3+Δ | 1735.8+Δ | 0.21(1) | | | | | | | (19/2) |
| 171.85(7) | 1614.1(2) | 1442.7(2) | 0.09(1) | | | | 0.74[e] | $d/q$ | 5/2 | 3/2 |
| 188.30(3) | 1615.7(3) | 1427.4(2) | 2.56(8) | 1.2(2) | −0.09(2) | −0.19(2) | 0.82[d] | $d/q$ | | $17/2^+$ |
| 193.39(3) | 1577.7(3) | 1384.5(2) | 2.72(8) | 0.7(2) | 0.0(2) | −0.1(2) | 0.95[i] | $E1$ | $1/2^-$ | $1/2^+$ |
| 215.84(8) | 1674.6(5) | 1458.7(2) | 0.12(1) | 0.9(3) | −0.34(6) | | | $d$ | 17/2 | 15/2 |
| 220.74(5) | 1679.1(2) | 1458.7(2) | 0.29(1) | | | | | | | 15/2 |
| 223.62(6) | 1839.1(4) | 1615.7(3) | 0.22(1) | | | | | | | |
| 228.73(4)[n] | 1409.5(1) | 1180.9(1) | 0.85(3) | | | | | | 11/2 | $13/2^+$ |
| 229.44(4) | 1656.9+Δ | 1427.5+Δ | 0.34(2) | 0.95(3) | −0.06(3) | | | ($d$) | (19/2) | (21/2) |
| 237.93(4)[n] | 1696.3(2) | 1458.7(2) | 0.41(2) | 1.41(1) | 0.29(3) | −0.06(3) | | $d$ | 15/2 | 15/2 |
| 245.71(4) | 1406.8(2) | 1160.5(1) | 0.82(4) | | | | | | 9/2 | $9/2^+$ |
| 249.07(4) | 1409.5(1) | 1160.5(1) | 0.62(2) | | | | 0.72[k] | $d/q$ | 11/2 | $9/2^+$ |
| 259.17(6) | 1994.9+Δ | 1735.8+Δ | 0.19(1) | | | | | | | (19/2) |
| 269.01(3) | 1696.3(2) | 1427.4(2) | 1.54(5) | 0.71(6) | −0.33(4) | −0.02(4) | 1.07[m] | $d/q$ | 15/2 | $17/2^+$ |
| 270.04(4)[n] | 1679.1(2) | 1409.5(1) | 1.09(4) | | | | | | 9/2 | 11/2 |
| 271.50(4) | 1730.2(4) | 1458.7(2) | 0.36(2) | | | | | | | 15/2 |
| 276.41(4) | 1436.7(2) | 1160.5(1) | 0.66(3) | | | | 0.85[k] | $d/q$ | 7/2 | $9/2^+$ |
| 277.87(3) | 1458.7(2) | 1180.9(1) | 8.1(2) | 1.25(7) | −0.37(4) | | 0.69[l] | $d$ | 15/2 | $13/2^+$ |
| 283.36(6)[n] | 1800.4(5) | 1517.0(2) | 0.22(1) | | | | | | | (7/2,9/2,11/2) |
| 285.70(3) | 1406.8(2) | 1121.5(1) | 3.36(11) | 0.88(4) | −0.25(5) | 0.20(5) | 0.66[j] | $d(/q)$ | 9/2 | 7/2 |
| 288.00(3) | 1409.5(1) | 1121.5(1) | 4.15(13) | 1.09(6) | 0.06(4) | −0.07(4) | | $q$ | 11/2 | 7/2 |
| 296.68(4) | 1739.1(3) | 1442.7(2) | 0.57(2) | 1.45(11) | 0.16(5) | 0.1(1) | 0.72[i] | $d/q$ | 5/2 | 3/2 |
| 308.35(3) | 1736.8+Δ | 1427.5+Δ | 2.31(7) | 0.89(1) | −0.23(4) | 0.0(1) | 0.85[m] | $d/q$ | 19/2 | (21/2) |
| 315.01(4) | 1436.7(2) | 1121.5(1) | 0.77(3) | 0.93(6) | −0.04(5) | −0.0(1) | | $d/q$ | 7/2 | 7/2 |
| 321.98(3)[n] | 1731.5(3) | 1409.5(1) | 2.15(7) | 1.06(2) | | | | $q$ | 7/2 | 11/2 |
| 334.54(3) | 1384.5(2) | 1050.2(2) | 7.2(2) | 1.13(2) | 0.09(3) | −0.05(3) | 1.00[i] | $q$ | 1/2 | $5/2^+$ |
| 345.29(18)[n] | 2077.0(3) | 1731.5(3) | 0.04(1) | 0.97(4) | 0.11(4) | −0.26(4) | | $q$ | 3/2 | 7/2 |
| 348.15(4) | 1508.5(2) | 1160.5(1) | 0.49(2) | | | | 0.81[k] | $d/q$ | (7/2) | $9/2^+$ |
| 354.61(4) | 1739.1(3) | 1384.5(2) | 0.63(2) | 1.02(4) | −0.1(5) | −0.0(1) | 1.14[i] | $q$ | 5/2 | $1/2^+$ |
| 355.25(5) | 2094.0(3) | 1739.1(3) | 0.23(1) | | | | | | | 5/2 |
| 356.61(3) | 1517.0(2) | 1160.5(1) | 1.77(6) | 1.27(4) | 0.06(4) | −0.0(1) | 0.80[k] | $d/q$ | (7/2,9/2,11/2) | $9/2^+$ |
| 358.81(3) | 1786.2(3) | 1427.4(2) | 1.49(5) | 1.28(4) | −0.15(5) | −0.1(1) | | $d/q$ | (19/2, 15/2) | $17/2^+$ |
| 363.17(3) | 1427.4(2) | 1064.4(1) | 55(2) | 0.83(1) | −0.27(3) | 0.03(3) | 0.78[f] | $d(/q)$ | $17/2^+$ | $15/2^-$ |
| 370.01(4)[n] | 1797.3(2) | 1427.4(2) | 0.86(3) | | | | | | 13/2 | $17/2^+$ |
| 377.73(3) | 1064.4(1) | 686.9(1) | 4.94(15) | 1.16(7) | 0.19(4) | −0.11(4) | 0.84[f] | $M2$ | $15/2^-$ | $11/2^+$ |
| 386.85(3) | 1508.5(2) | 1121.5(1) | 2.58(9) | 1.02(6) | 0.05(4) | −0.01(4) | 0.88[j] | $d$ | 7/2 | $7/2^+$ |
| 392.50(3) | 1442.7(2) | 1050.2(2) | 7.5(2) | 0.98(6) | 0.01(3) | 0.00(3) | 0.95[i] | $d/q$ | 3/2 | $5/2^+$ |
| 406.67(9) | 1816.2(7) | 1409.5(1) | 0.16(1) | | | | | | | 11/2 |
| 411.50(7)[n] | 1839.1(4) | 1427.4(2) | 0.21(1) | | | | | | | $17/2^+$ |
| 415.18(8)[n] | 2292.1(5) | 1876.8(3) | 0.11(1) | | | | | | 9/2 | 11/2 |
| 424.79(4) | 2040.5(4) | 1615.7(3) | 0.58(2) | 0.81(6) | −0.30(4) | 0.05(5) | 1.05[m] | $d/q$ | (15/2, 19/2) | $17/2^+$ |
| 434.96(8)[n] | 2448.0(6) | 2013.0(3) | 0.14(1) | 1.23(15) | 0.22(6) | −0.01(7) | | $d$ | 11/2 | 11/2 |
| 444.20(4)[n] | 2457.2(4) | 2013.0(3) | 0.81(3) | 0.83(5) | −0.18(4) | −0.06(4) | | $d$ | 13/2 | 11/2 |
| 445.61(6)[n] | 2023.0(3) | 1577.7(3) | 0.11(1) | | | | | | 1/2 | $1/2^-$ |
| 455.43(5)[n] | 2032.7(3) | 1577.7(3) | 0.14(1) | | | | | | 1/2 | $1/2^-$ |
| 458.17(5) | 1508.5(2) | 1050.2(2) | 0.67(3) | 0.77(6) | −0.25(4) | −0.07(4) | 0.68[i] | $d$ | 7/2 | 5/2 |

TABLE I. (*Continued.*)

| $\gamma$-ray energy $E_\gamma$ (keV) | Initial state $E_i$ (keV) | Final state $E_f$ (keV) | Intensity $I_\gamma$ | Anisotropy $A$ | Angular $A_2/A_0$ | distribution $A_4/A_0$ | ADO | Multi-polarity | $I_i^\pi$ | $I_f^\pi$ |
|---|---|---|---|---|---|---|---|---|---|---|
| 462.93(4) | 2077.0(3) | 1614.1(2) | 0.54(2) | 0.89(6) | −0.14(4) | 0.08(4) | | $d$ | 3/2 | 5/2 |
| 473.60(5)[n] | 1160.5(1) | 686.9(1) | 0.57(3) | 0.91(7) | −0.02(5) | 0.20(5) | 0.92[f] | $q$ | $9/2^+$ | $11/2^+$ |
| 475.00(4) | 1902.5+Δ | 1427.5+Δ | 0.56(2) | 0.95(6) | 0.06(4) | 0.21(4) | | $d/q$ | (23/2) | (21/2) |
| 476.34(4)[n] | 1597.7(8) | 1121.5(1) | 1.32(5) | | | | | | (13/2) | $7/2^+$ |
| 477.63(5) | 1637.8(2) | 1160.5(1) | 0.40(2) | 0.81(8) | −0.45(6) | 0.16(7) | | $d/q$ | 11/2 | $9/2^+$ |
| 486.35(4) | 1913.8(3) | 1427.4(2) | 0.70(3) | 0.90(7) | 0.13(4) | −0.30(5) | | $q$ | 21/2 | $17/2^+$ |
| 492.54(4) | 1614.1(2) | 1121.5(1) | 1.78(6) | 0.76(5) | −0.22(3) | −0.07(3) | 0.87[j] | $d/q$ | 5/2 | $7/2^+$ |
| 494.05(3) | 1180.9(3) | 686.9(1) | 1.50(5) | | | | 0.90[f] | $q$ | $13/2^+$ | $11/2^+$ |
| 503.23(7)[n] | 1930.6(5) | 1427.4(2) | 0.26(2) | 1.1(2) | −0.03(2) | 0.28(17) | | $q$ | 19/2 | 17/2 |
| 514.98(4)[n] | 1696.3(2) | 1180.9(1) | 3.08(10) | 1.4(3) | −0.1(2) | 0.1(2) | 0.89[l] | $q$ | 15/2 | 13/2 |
| 516.14(3) | 1637.8(2) | 1121.5(1) | 2.80(9) | | | | 0.81[j] | $d/q$ | (11/2) | $7/2^+$ |
| 521.79(13)[n] | 1682.6(4) | 1160.5(1) | 0.11(1) | 0.93(13) | −0.23(7) | 0.30(9) | | $d/q$ | (7/2) | $9/2^+$ |
| 533.69(4) | 1583.9(3) | 1050.2(2) | 1.68(6) | 1.05(3) | 0.09(4) | 0.02(4) | 0.76[i] | $d/q$ | (5/2) | $5/2^+$ |
| 537.58(6)[n] | 2578.0(6) | 2040.5(4) | 0.21(1) | | | | | | | (15/2,19/2) |
| 550.90(5) | 1978.4+Δ | 1427.5+Δ | 0.52(2) | 1.34(7) | 0.56(5) | 0.01(6) | | $d$ | (21/2) | (21/2) |
| 557.31(4)[n] | 1679.1(2) | 1121.5(1) | 1.44(5) | 0.91(6) | 0.03(6) | 0.34(7) | 0.84[j] | $d/q$ | 9/2 | $7/2^+$ |
| 563.83(4) | 1614.1(2) | 1050.2(2) | 1.58(6) | 1.09(8) | | | 0.95[i] | $d$ | 5/2 | $5/2^+$ |
| 587.41(5)[n] | 1637.8(2) | 1050.2(2) | 0.72(3) | | | | | | | $5/2^+$ |
| 604.85(4)[n] | 1726.4(2) | 1121.5(1) | 2.05(7) | | | | | | 7/2 | $7/2^+$ |
| 634.27(6)[n] | 2093.0(5) | 1458.7(2) | 0.34(2) | | | | | | | 15/2 |
| 645.50(3) | 2223.2(4) | 1577.7(3) | 1.05(3) | 0.9(2) | −0.1(1) | −0.3(1) | 0.91[a] | $q$ | $5/2^-$ | $1/2^-$ |
| 651.05(4) | 2094.0(3) | 1442.7(2) | 0.50(2) | | | | | | | 3/2 |
| 654.33(6)[n] | 1814.8(3) | 1160.5(1) | 0.42(2) | | | | | | 11/2 | $9/2^+$ |
| 665.62(3) | 2093.0(3) | 1427.4(2) | 2.93(9) | 1.3(2) | 0.24(7) | | 0.61[d] | $d$ | 17/2 | $17/2^+$ |
| 668.47(5) | 2111.2(2) | 1442.7(2) | 0.36(2) | | | | | | | 3/2 |
| 674.68(7)[n] | 2111.2(2) | 1436.7(2) | 0.30(2) | | | | | | | 7/2 |
| 676.26(4) | 2103.7+Δ | 1427.5+Δ | 0.85(3) | | | | | | | (21/2) |
| 686.79(3) | 686.9(1) | 0.0 | 40.6(3) | 1.32(3) | 0.07(4) | −0.03(3) | 0.85[d] | $(d/q)$ | $11/2^+$ | $9/2^+$ |
| 693.32(6)[n] | 1814.8(3) | 1121.5(1) | 0.56(3) | | | | | | 11/2 | $7/2^+$ |
| 694.05(6)[n] | 2152.8(5) | 1458.7(2) | 0.34(2) | | | | | | | 15/2 |
| 725.49(4)[n] | 2152.9(3) | 1427.4(2) | 1.36(5) | | | | 0.73[d] | $d/q$ | (19/2,15/2) | $17/2^+$ |
| 734.48(6)[n] | 2144.2(3) | 1409.5(1) | 0.39(2) | | | | | | | 11/2 |
| 736.54(4)[n] | 1917.4(2) | 1180.9(1) | 2.35(9) | 0.66(7) | −0.12(4) | −0.04(6) | 0.49[l] | $d$ | (11/2, 9/2) | $13/2^+$ |
| 755.28(4)[n] | 1876.8(3) | 1121.5(1) | 1.17(5) | | | | 1.00[j] | $d$ | 11/2 | $7/2^+$ |
| 758.41(4) | 2185.9+Δ | 1427.5+Δ | 1.27(4) | | | | 1.03[d] | $q$ | (25/2) | (21/2) |
| 760.60(18)[n] | 1921.(1) | 1160.5(1) | 0.10(1) | 1.34(12) | 0.02(5) | 0.65(6) | | $q$ | 11/2 | $9/2^+$ |
| 781.27(9) | 2208.7(6) | 1427.4(2) | 0.26(2) | 1.2(2) | 0.0(1) | | | $d$ | 17/2 | 17/2 |
| 790.44(5) | 2217.9(4) | 1427.4(2) | 0.58(2) | 0.8(2) | −0.1(1) | | | $d$ | 19/2 | 17/2 |
| 795.89(4)[n] | 1917.4(2) | 1121.5(1) | 2.45(9) | 0.9(2) | −0.37(1) | 0.36(2) | 0.92[j] | | (11/2, 9/2) | $7/2^+$ |
| 822.79(8)[n] | 2259.2(3) | 1436.7(2) | 0.27(2) | | | | | | | 7/2 |
| 829.72(5)[n] | 1517.0(2) | 686.9(1) | 1.02(4) | | | | | | (7/2,9/2,11/2) | $9/2^+$ |
| 832.00(9)[n] | 2013.0(3) | 1180.9(1) | 0.51(3) | | | | | | 11/2 | $13/2^+$ |
| 846.04(1)[n] | 2006.5(9) | 1160.5(1) | 0.20(2) | | | | | | | $11/2^+$ |
| 852.88(4)[n] | 2311.6(4) | 1458.7(2) | 0.92(3) | | | | | | | (15/2) |
| 854.26(4) | 2296.9(3) | 1442.7(2) | 1.03(4) | | | | 0.70[e] | $d/q$ | (5/2, 1/2) | 3/2 |
| 895.81(4) | 2338.5(4) | 1442.7(2) | 0.87(3) | 0.75(1) | −0.27(4) | 0.06(4) | 1.18[e] | $d/q$ | (5/2) | 3/2 |
| 904.60(4)[n] | 2332.0(4) | 1427.4(2) | 0.85(3) | | | | | | | $17/2^+$ |
| 906.31(5) | 2027.8(4) | 1121.5(1) | 1.07(5) | | | | | | | $7/2^+$ |
| 910.69(4)[n] | 2719.3(4) | 1808.6(3) | 0.99(4) | | | | 0.77[f] | $d/q$ | | (13/2, 9/2) |
| 913.20(4)[n] | 2340.6(3) | 1427.4(2) | 0.98(2) | | | | 1.19[d] | $q$ | (21/2, 13/2) | $17/2^+$ |
| 914.99(5) | 2299.5(4) | 1384.5(2) | 0.51(2) | | | | 1.16[c] | $q$ | 5/2 | $1/2^+$ |
| 924.87(4) | 2352.5(3) | 1427.4(2) | 1.20(4) | | | | 1.02[d] | $q$ | (21/2, 13/2) | $17/2^+$ |
| 928.83(13)[n] | 2050.4(9) | 1121.5(1) | 0.25(2) | | | | | | | $7/2^+$ |
| 948.54(3)[n] | 2013.0(3) | 1064.4(1) | 3.40(12) | 1.07(3) | 0.35(4) | −0.01(4) | | $q$ | 11/2 | $15/2^-$ |
| 969.01(4) | 2546.7(4) | 1577.7(3) | 0.39(1) | | | | | | $(3/2^-)$ | $1/2^-$ |
| 972.59(4) | 2023.0(3) | 1050.2(2) | 1.70(6) | | | | 0.93[i] | $q$ | 1/2 | $5/2^+$ |

TABLE I. (*Continued.*)

| $\gamma$-ray energy $E_\gamma$ (keV) | Initial state $E_i$ (keV) | Final state $E_f$ (keV) | Intensity $I_\gamma$ | Anisotropy $A$ | Angular $A_2/A_0$ | distribution $A_4/A_0$ | ADO | Multi-polarity | $I_i^\pi$ | $I_f^\pi$ |
|---|---|---|---|---|---|---|---|---|---|---|
| 982.15(5) | 2032.7(3) | 1050.2(2) | 1.32(5) | | | | 0.87[i] | $q$ | 1/2 | $5/2^+$ |
| 988.38(11)[n] | 2148.8(8) | 1160.5(1) | 0.23(2) | | | | | | | $9/2^+$ |
| 991.67(4)[n] | 1679.1(2) | 686.9(1) | 1.38(5) | 2.0(7) | | | 0.61[f] | $d$ | 9/2 | $11/2^+$ |
| 1002.95(6) | 2430.4(5) | 1427.4(2) | 0.47(2) | | | | | | | 17/2 |
| 1008.96(7)[n] | 1696.3(2) | 686.9(1) | 0.54(3) | | | | | | 15/2 | $11/2^+$ |
| 1014.17(15) | 2473(1) | 1458.7(2) | 0.14(1) | | | | | | | 15/2 |
| 1014.70(4) | 2443.2+$\Delta$ | 1427.5+$\Delta$ | 0.94(4) | 0.83(1) | −0.26(3) | 0.10(3) | | $d/q$ | (23/2, 19/2) | (21/2) |
| 1026.58(5)[n] | 2076.8(4) | 1050.2(2) | 1.34(5) | | | | | | | $5/2^+$ |
| 1028.39(3) | 1715.3(3) | 686.9(1) | 5.0(2) | 1.09(1) | 0.33(4) | 0.01(3) | 0.63[f] | $d$ | (9/2, 13/2) | $11/2^+$ |
| 1028.79(5)[n] | 2189.4(3) | 1160.5(1) | 1.17(5) | | | | | | | $9/2^+$ |
| 1039.56(4) | 1726.4(2) | 686.9(1) | 2.55(9) | | | | 1.01[f] | $q$ | 7/2 | $11/2^+$ |
| 1044.76(6)[n] | 2166.3(4) | 1121.5(1) | 0.95(4) | | | | | | | $7/2^+$ |
| 1050.20(3) | 1050.2(2) | 0.0 | 32.9(3) | 0.87(1) | −0.09(3) | −0.0(3) | 0.81[c] | $E2$ | $5/2^+$ | $9/2^+$ |
| 1060.87(4) | 2111.2(2) | 1050.2(2) | 3.12(11) | | | | | | | $5/2^+$ |
| 1064.28(3) | 1064.4(1) | 0.0 | 100(3) | 1.16(1) | 0.33(3) | −0.00(3) | | $E3$ | $15/2^-$ | $9/2^+$ |
| 1110.23(3) | 1797.3(2) | 686.9(1) | 4.18(14) | 1.21(2) | 0.42(4) | −0.11(3) | 0.59[f] | $d$ | 13/2 | $11/2^+$ |
| 1121.54(4) | 1121.5(1) | 0.0 | 36.5(3) | 1.00(1) | 0.18(3) | 0.03(3) | 0.78[g] | $d/q$ | $7/2^+$ | $9/2^+$ |
| 1121.64(4) | 1808.6(3) | 686.9(1) | 1.94(7) | | | | 0.59[f] | $d$ | (13/2, 9/2) | $11/2^+$ |
| 1127.70(6)[n] | 1814.8(3) | 686.9(1) | 0.71(3) | | | | 0.98[f] | $d$ | 11/2 | $11/2^+$ |
| 1131.87(11)[n] | 2292.1(5) | 1160.5(1) | 0.25(2) | 1.45(8) | | | | $d$ | 9/2 | $9/2^+$ |
| 1137.46(6)[n] | 2259.2(3) | 1121.5(1) | 0.93(4) | 1.05(8) | −0.01(5) | | | | | $7/2^+$ |
| 1155.19(9)[n] | 2276.7(7) | 1121.5(1) | 0.41(3) | | | | | | | $7/2^+$ |
| 1160.41(3) | 1160.5(1) | 0.0 | 15(1) | 0.75(1) | −0.15(3) | −0.02(3) | 0.77[h] | $d/q$ | $9/2^+$ | $9/2^+$ |
| 1180.94(3) | 1180.9(1) | 0.0 | 46(2) | 1.04(1) | 0.24(3) | | 1.08[b] | $q$ | $13/2^+$ | $9/2^+$ |
| 1188.63(4)[n] | 2253.0(3) | 1064.4(1) | 2.69(10) | | | | | | | $15/2^-$ |
| 1190.11(4) | 1877.0(3) | 686.9(1) | 1.93(7) | | | | 0.73[f] | $d/q$ | (13/2, 9/2) | $11/2^+$ |
| 1214.50(8)[n] | 2375.1(7) | 1160.5(1) | 0.46(3) | | | | | | | $9/2^+$ |
| 1226.83(5) | 2277.1(4) | 1050.2(2) | 1.27(5) | 1.0(7) | −0.3(3) | | | ($d$) | (7/2, 3/2) | $5/2^+$ |
| 1250.11(4)[n] | 2314.5(4) | 1064.4(1) | 2.86(10) | 0.58(3) | −0.23(5) | 0.55(5) | | ($q$) | (17/2) | $15/2^-$ |
| 1253.54(9)[n] | 2375.1(7) | 1121.5(1) | 0.44(3) | | | | | | | $7/2^+$ |
| 1257.52(4) | 1944.4(3) | 686.9(1) | 4.29(14) | 0.89(3) | 0.53(4) | −0.07(4) | 0.92[f] | $q$ | 15/2 | $11/2^+$ |
| 1277.43(12)[n] | 2399.0(9) | 1121.5(1) | 0.30(2) | 0.90(4) | −0.07(4) | | | $d$ | 5/2 | $7/2^+$ |
| 1288.36(4)[n] | 2352.8(3) | 1064.4(1) | 2.06(8) | 0.96(7) | 0.2(1) | −0.1(2) | | $q$ | 11/2 | $15/2^-$ |
| 1301.66(6)[n] | 2351.9(4) | 1050.2(2) | 0.95(4) | 1.7(2) | 0.4(1) | | | $d$ | 5/2 | $5/2^+$ |
| 1341.90(5)[n] | 2406.3(4) | 1064.4(1) | 1.34(6) | 1.00(7) | −0.09(9) | | | $d$ | 13/2 | $15/2^-$ |
| 1355.33(5)[n] | 2042.3(4) | 686.9(1) | 1.35(5) | 0.8(7) | −0.0(1) | −0.4(3) | | | | $11/2^+$ |
| 1360.70(2)[n] | 2482.(1) | 1121.5(1) | 0.19(2) | | | | | | | $7/2^+$ |
| 1384.07(5)[n] | 2448.4(4) | 1064.4(1) | 1.49(6) | 0.76(14) | −0.04(4) | | | $d$ | (13/2, 17/2) | $15/2^-$ |
| 1407.30(39) | 1406.8(2) | 0.0 | 2.3(4)[s] | 1.4(3) | 0.43(9) | | | $d$ | 9/2 | $9/2^+$ |
| 1409.73(4) | 1409.5(1) | 0.0 | 10.0(4) | 0.8(2) | −0.26(5) | 0.18(5) | | | 11/2 | $9/2^+$ |
| 1437.27(7) | 1436.7(2) | 0.0 | 7.1(8) | 0.91(1) | 0.09(3) | −0.03(3) | | ($q$) | 7/2 | $9/2^+$ |
| 1457.45(5)[n] | 2144.2(3) | 686.9(1) | 1.35(5) | | | | | | | $11/2^+$ |
| 1462.90(5)[n] | 2149.8(4) | 686.9(1) | 1.40(5) | 0.94(6) | −0.02(4) | −0.13(5) | | ($q$) | | $11/2^+$ |
| 1478.44(8)[n] | 2599.9(5) | 1121.5(1) | 0.58(3) | | | | | | | $7/2^+$ |
| 1503.45(1)[n] | 2189.4(3) | 686.9(1) | 0.30(2) | | | | | | | $11/2^+$ |
| 1517.86(9)[n] | 1517.01(20) | 0.0 | 3.3(3) | 0.83(12) | 0.01(6) | −0.11(9) | | $d/q$ | (7/2,9/2,11/2) | $9/2^+$ |
| 1549.78(15) | 2599.9(5) | 1050.2(2) | 0.24(2) | | | | | | | $5/2^+$ |
| 1583.90(21)[n] | 1583.9(3) | 0.0 | 0.62(8)[s] | | | | | | (5/2) | $9/2^+$ |
| 1592.76(15)[n] | 2753.(1) | 1160.5(1) | 0.19(2) | | | | | | | $9/2^+$ |
| 1597.74(8)[n] | 2662.1(6) | 1064.4(1) | 0.80(4) | | | | | | | $15/2^-$ |
| 1626.39(9)[n] | 2313.3(7) | 686.9(1) | 0.47(3) | | | | | | | $11/2^+$ |
| 1636.86(6)[n] | 2701.2(5) | 1064.4(1) | 1.24(6) | | | | | | | $15/2^-$ |

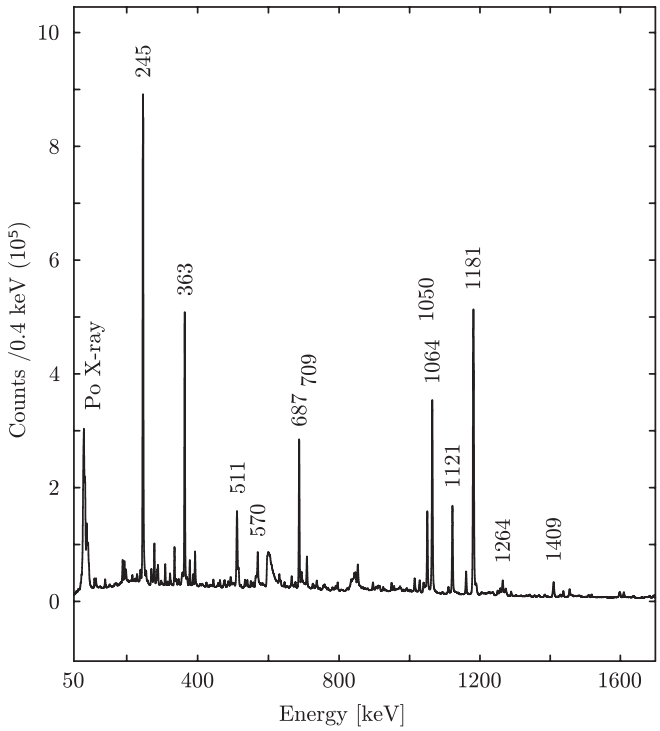


FIG. 1. The total projection spectrum of the $E_\gamma$-$E_\gamma$ matrix. Only the most prominent peaks are marked with their energies. The presence of the $^{210}$Po nucleus is seen by the 245-keV peak and partly the 1181-keV peak while the $^{207}$Pb nucleus is noted by the 570-keV peak.

2578 keV, above the 2041-keV level with the de-exciting 425-keV transition; see Fig. 2.

Figure 6(b) shows the gate of 1064-keV transition decaying from the $15/2^-$ level at 1064 keV to the ground state. Perhaps the first notable change compared to the gate of 363 keV in Fig. 6(a) are the transitions 1189, 1250, 1288, 1342, 1384, and 1598 keV. These new transitions, among others, will be discussed more in Sec. IV and their placement in the level scheme can be seen in Fig. 3. As the 570-keV transition in $^{207}$Pb, the decay product of $^{211}$Po, also has a coincident 1064-keV peak [20], it is also present in Fig. 6(b). In the same gated spectrum, the 269- and 270-keV peak is a doublet consisting of both the 269- and 270-keV transitions originating from the 1679- and 1696-keV levels, respectively.

The gate of the 687-keV transition from the $11/2^+$ level at 687 keV can be seen in Fig. 6(c). Only the most intense $\gamma$ transitions from Fig. 6(b) are seen in Fig. 6(c) as the branching at the $15/2^-$ level at 1064 keV heavily favors the decay path down to the ground state compare to the decay to the $11/2^+$ level at 687 keV. Other changes include the transitions that appear in almost two groupings, i.e., the first roughly 1030 to 1258 keV and the second one from 1355 to 1626 keV. The $\gamma$-ray transitions from these groups and their initial levels can be seen in the partial level scheme in Fig. 3.

The doublet at 474 and 475 keV in Fig. 6(c) consists of both a new transition at 474 keV, originating from the $9/2^+$ level at 1160 keV shown in Fig. 3, and a known transition at 475 keV between the levels $1902 + \Delta$ keV and $1427 + \Delta$ keV [9]. The 475-keV transition is also seen in Figs. 6(b) and 6(a). When comparing the different gates in Fig. 6, the gate of 687 keV displays mainly energetically higher $\gamma$ rays while the gate of 363 keV show less energetic $\gamma$ rays. The gate on 1064 keV, on the other hand, displays both low- and high-energy $\gamma$ rays. Most of the peaks shown in Fig. 6(a) are also found in Fig. 6(b).

Figure 7(a) shows the gate of the 1160-keV $\gamma$-ray transition and in the right-hand side of Fig. 5 the partial level scheme of the most of the levels decaying down to the $9/2^+$ level at 1160 keV are shown. The 1160-keV gate in Ref. [7] was relatively empty with a few transitions at the lower end of the spectrum, while in current work, the majority of peaks in Fig. 7(a) are new. In Fig. 7(a), the 245- and 249-keV peaks are almost on top of each other. The 245-keV peak is a coincidence from $^{210}$Po while the 249-keV peak is the transition between the levels at 1409 and 1160 keV.

The 1122-keV gate is shown in Fig. 7(b) and the corresponding level scheme shown in the middle part of Fig. 5 is constructed with most of the new transitions seen in this gate. The transitions 286 and 288 keV in Fig. 7(b) are hard to distinguish and seem to make the total peak broader. These transitions originate from the levels at 1407 and 1409 keV, respectively, and are shown, for instance, in Fig. 4.

In Fig. 7(c), the gate of 1050 keV is shown and the left-hand side of the partial level scheme in Fig. 4 shows most of the $\gamma$-ray transitions in coincidence with the 1050-keV

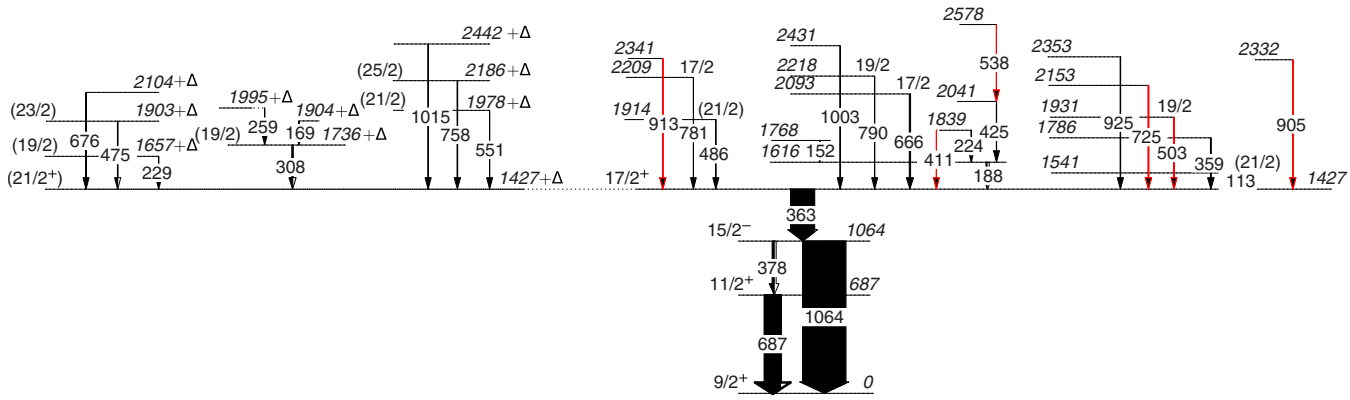


FIG. 2. Partial level scheme showing the decay of levels above the 1427-keV and $1427+\Delta$ levels. New transitions are marked in red.

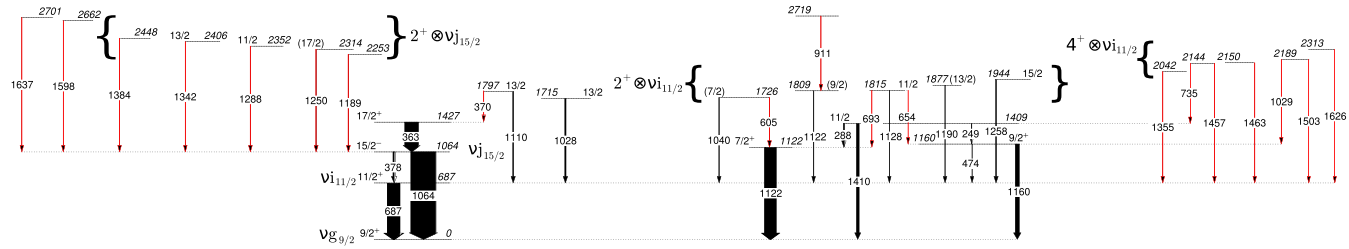

FIG. 3. Partial level scheme portraying mainly the $\pi(h_{9/2})^2_{2+} \otimes \nu i_{11/2}$, $\pi(h_{9/2})^2_{4+} \otimes \nu i_{11/2}$, and $\pi(h_{9/2})^2_{2+} \otimes \nu j_{15/2}$ multiplets. New transitions are marked in red.

transition. Certain peaks higher up in energy than 1227 keV in Fig. 7(c) are not placed in current level schemes, for instance, the 1274- and 1389-keV transitions, as gates on these peaks neither have enough statistics nor yield transitions to draw explicit conclusions from.

Comparing the transitions 534 keV and 564 keV, from the levels 1584 and 1614 keV, respectively, in Fig. 7(c) with the gate of 1050 in Fig. 6, in Ref. [7], one can see that the intensities have switched so that in the present study the 534-keV peak is now the larger one. This would indicate that the 1584-keV level either has a higher or the same spin value than the 1614-keV level and/or that the level feeding the 1614-keV level has a low spin value.

With a slightly lower measured energy for the 458-keV transition and slightly higher energies for the 348- and 387-keV transitions, these $\gamma$ rays were placed to originate from the same level at 1508 keV as opposed to two different levels at 1508 and 1509 keV as reported in Ref. [7]. There are two other instances where the two level energies are very close to one another. In the first case, the levels of interest are the levels at 1876.8(3) and 1877.0(5) keV, and in the second case, it is the levels at 2152.8(5) and 2152.9(3) keV. In the first case, the levels are assigned different spin values and are thereby clearly two different levels, see Table I, while the spin values are inconclusive in the other case and it remains unknown whether they are the same level or not.

The 1518-keV $\gamma$-ray transition is assigned to originate from the level at 1517 keV even though there is a slight discrepancy between the $\gamma$-ray energy and the energy of the level in question. The placement of the 1518-keV $\gamma$ ray is based upon the coincident $\gamma$ rays of the 166 and 283 keV that are also seen by the 357-keV transition from the 1517-keV level.

### B. Level spin assignment

Not all levels with $\gamma$-ray transitions, with measured angular data, alone were conclusive regarding their level spin. It is possible to draw conclusions regarding the involved spins by looking at the levels connected by transitions both to and from the levels in question. In this subsection, the arguments for some of these assignments will be discussed in detail.

The spin of the levels 1443 and 1614 keV are determined at the same time, from both the decay of these levels and from the feeding decay connected to these levels; see Fig. 4. The 392-keV transition between the 1443-keV level and the $5/2^+$ level at 1050 keV has a measured ADO value of 0.95, and the angular distribution values are close to being isotropic in nature. Looking at the ADO value, the spin for the 1443-keV level is either $9/2$ or $1/2$ with a stretched quadrupole transition, $5/2$ as $\Delta J = 0$ transition, and $3/2$ or $7/2$ as mixed $\Delta J = 1$ transition. The levels 1443 and 1614 keV are also connected through a mixed $\Delta J = 1$ 172-keV transition and the 1614-keV level also decays to the $7/2^+$ level at 1122 keV with a mixed $\Delta J = 1$ 493-keV transition and to the $5/2^+$ level at 1050 keV with a 564-keV transition with an ADO value of 0.95. The only possible spin values to satisfy all the end spins for the known 1050- and 1122-keV levels and the spin differences from the $\gamma$-ray transitions are $3/2$ or $7/2$ for the 1443-keV level and $5/2$ for the 1614-keV level with the 392-keV transition being a mixed $\Delta J = 1$ and the 564 keV being a $\Delta J = 0$ transition. Out of the two possible spin values for the 1443-keV level, the $3/2$ is considered to be the more likely one, as a with a spin value of $7/2$ one would also expect decay to the $9/2$ level at 1160 keV.

The ADO value of the 992-keV transition between the level at 1679 keV, shown in Fig. 5, and the $11/2^+$ level at 687 keV

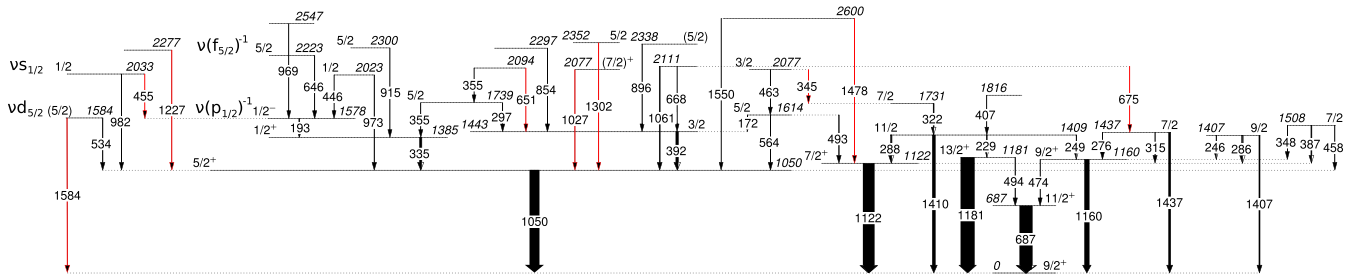

FIG. 4. Partial level scheme depicting mainly the decay of levels above and connected the 1050-keV level. New transitions are marked in red.

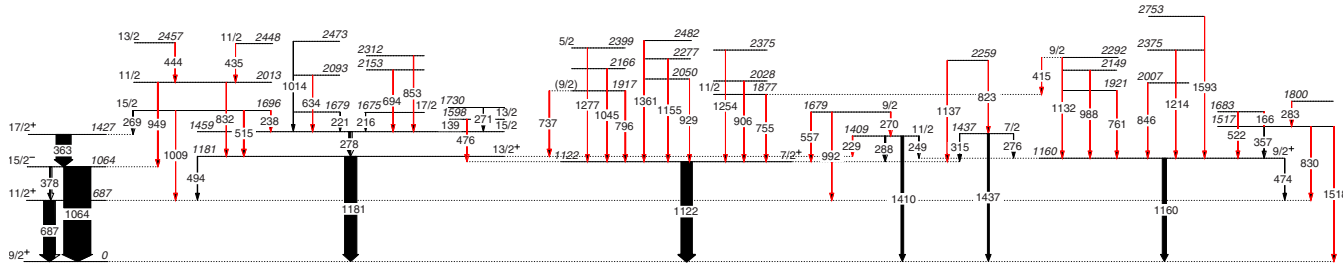

FIG. 5. Partial level scheme displaying transitions cascading through the 1181, 1122-, and 1160-keV levels. New transitions are marked in red.

is indicated as being a stretched dipole transition giving the transmitting level the possible spins of 9/2 and 13/2. The 557-keV transition between the same 1679-keV level and the $7/2^+$ level at 1122 keV is a mixed $\Delta J = 1$ transition, thereby eliminating the possibility of the 1679-keV level from having the spin value of 13/2.

The measured anisotropy of the 522-keV transition, decaying from the level at 1683 keV to the $9/2^+$ level at

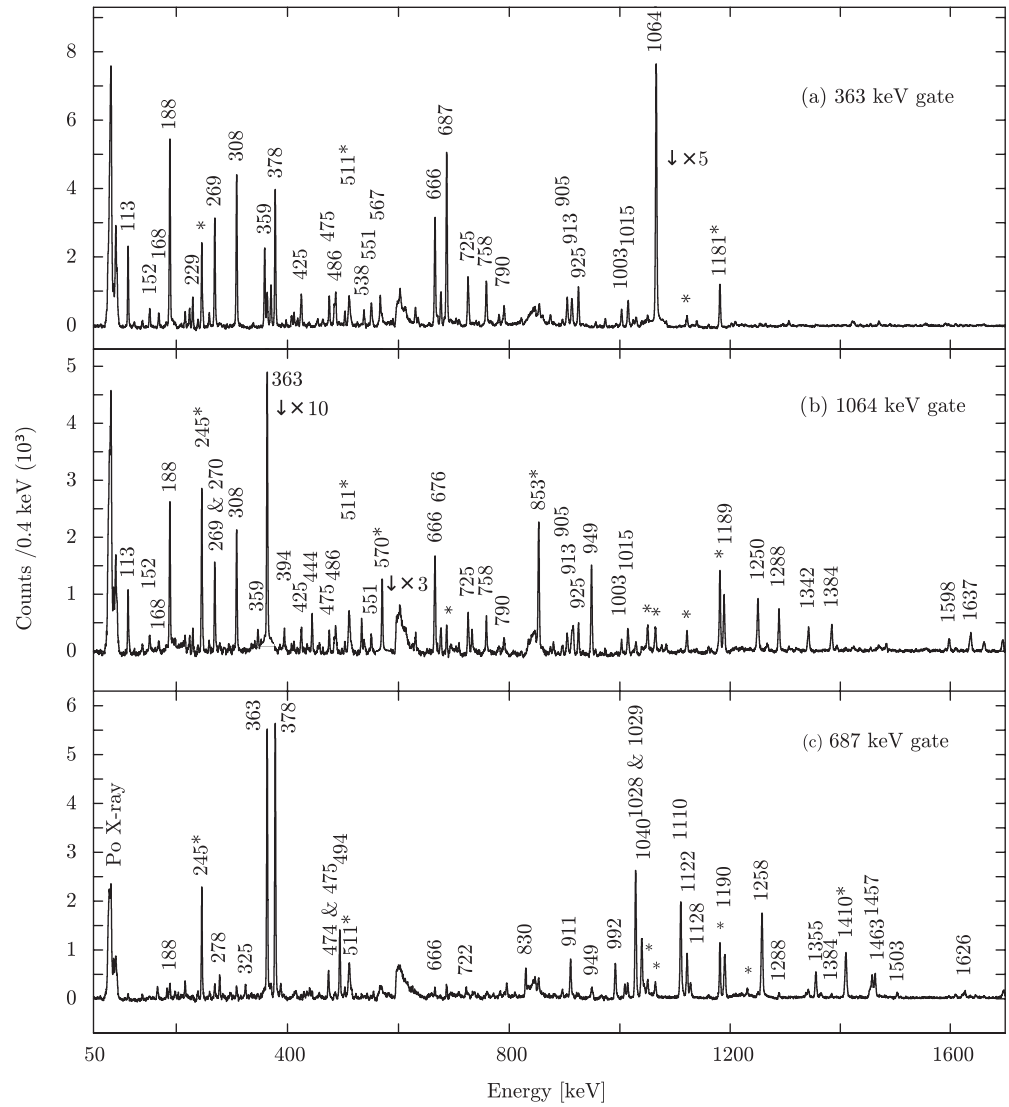


FIG. 6. Spectra obtained from the $E_\gamma$-$E_\gamma$ matrix of prompt transitions measured by JUROGAM I gated with selected transitions in $^{211}$Po. Prominent transitions are marked with their energies in units of keV while chance coincidences and contaminants are marked with an asterisk. The transitions 363 and 570 keV in the 1064-keV gate and the 1064-keV transition in the 363-keV gate have been downsized by the amount indicated next to the peak in question.

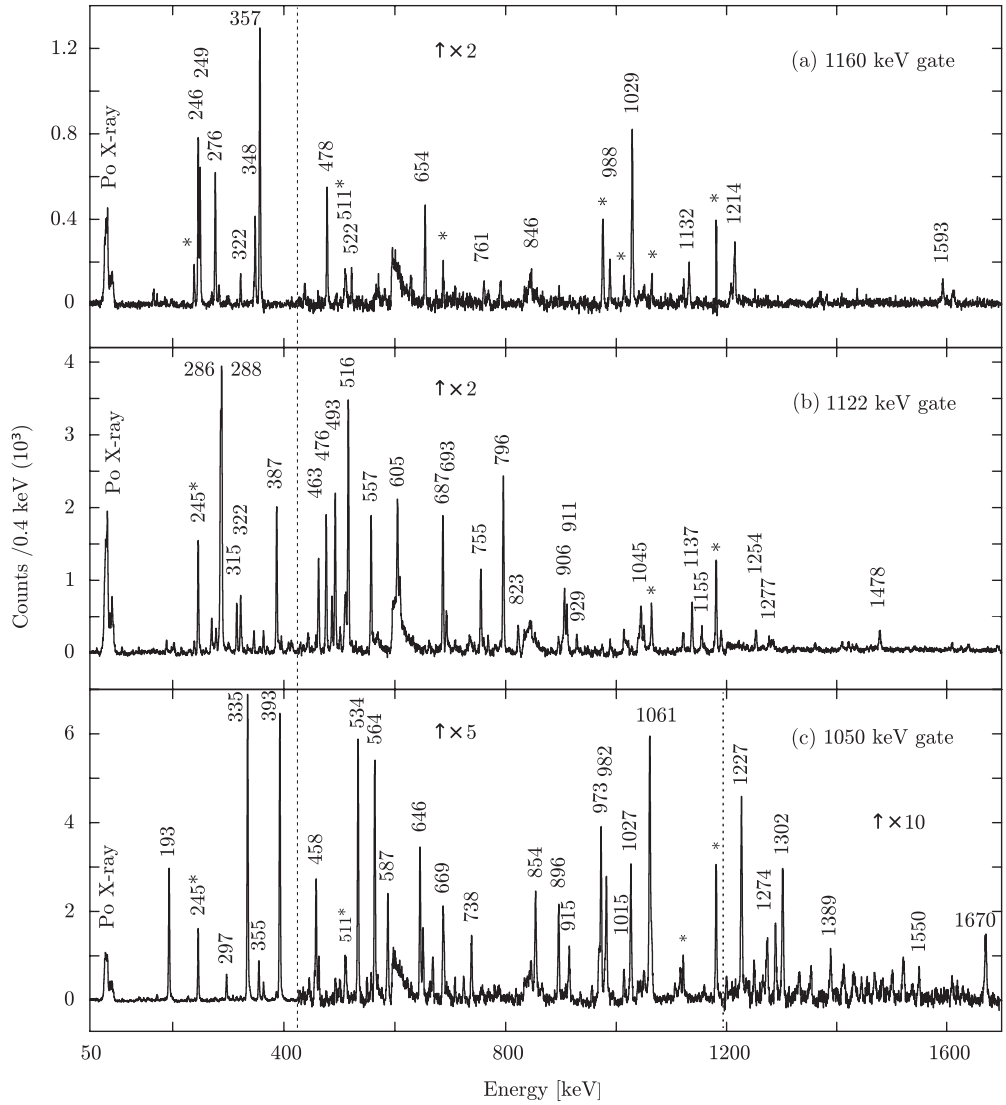


FIG. 7. Spectra were obtained from the $E_\gamma$-$E_\gamma$ matrix gated with selected transitions in $^{211}$Po. Prominent transitions are marked with their energies in units of keV while chance coincidences and contaminants are marked with an asterisk. The scaled regions are marked by dashed lines and the amount of scaling done is shown by the corresponding number next to the arrows.

1160 keV, shown in Fig. 5, indicates that it is a stretched pure quardupole transition. Besides the rather large $A_4/A_0$ value, the angular distribution would suggest that the 522-keV transition is an upward nonstretched quadrupole transition. Leaning more toward the angular distribution and considering the above-mentioned ambiguity, the 1683-keV level is tentatively assigned the spin value of (7/2). The level at 1696 keV, to the left in Fig. 5, is given the spin value of 15/2 as two of three transitions, 269 keV to the 17/2 level at 1427 keV and 515 keV to the 13/2 level at 1181 keV, from this level have the measured values of $d/q$ transitions. As the third 1008-keV transition does not contribute to the 1696-keV level assignment, the spin value is given based only on the two first transitions.

The level at 1726 keV, shown in the center of Fig. 3, decays both to the $7/2^+$ level at 1122 keV with a 605-keV transition and to the $11/2^+$ level at 687 keV with a 1040-keV transition. With the 1040-keV $\gamma$ ray being a stretched quadrupole transition, the level at 1726 keV has the possible spin values of either 7/2 or 15/2. The spin value of 7/2, rather than 15/2, is more favorable for the conditions set up by the decay to the $7/2^+$ level at 1122 keV to be fulfilled.

With an ADO value of 0.98, the 1128-keV transition gives the following possible spin values of 7/2 or 15/2 as a stretched quadrupole transition and 11/2 as a $\Delta J = 0$ transition for the level at 1815 keV. The 1815-keV level also decays to the $7/2^+$ and $9/2^+$ levels, at 1122 and 1160 keV respectively, which rules out the spin value of 15/2, and while 7/2 is possible, one would in that case also expect a transition to the $5/2^+$ level at 1050 keV. Therefore, the level at 1815 keV is assigned the spin value of 11/2.

The transitions originating from the 1917-keV level, i.e., the 737-keV transition to the $13/2^+$ level at 1180 keV and the 796-keV transition to the $7/2^+$ level at 1122 keV, see middle of Fig. 5, are somewhat problematic with the current data at hand. Working with mostly dipole and quadrupole transitions,

the spin values for the 1917-keV level should be either $9/2$ or $11/2$. Ignoring the very low ADO value for the 737-keV transition, the other distribution values show properties of an upward dipole transition, indicating that the 1917-keV level should have a spin value of $11/2$. On the other hand, the analysis of the properties of the 796-keV transition shows that it is a $\Delta J = 1$ mixed transition and out of the two possible spin values, for the 1917-keV level, the $9/2$ works best in this case. With conflicting evidence, the 1917-keV level is marked as either $11/2$ or $9/2$.

The ADO value for the 973-keV $\gamma$-ray transition between the 2023- and 1050-keV levels proposes a stretched quardupole transition, i.e., initial level as either $9/2$ or $1/2$. The spin value for the 2023-keV level is then set as $1/2$ as it also decays to the $1/2^-$ level at 1578 keV; see Fig. 4.

A spin value of $1/2$ was assigned to the level at 2033 keV shown in the right-hand side of Fig. 4 as the transition from this level to the 1050-keV level and is a stretched quadrupole, while the new transition at 455 keV, also from the 2033-keV level, decays to the $1/2^-$ level at 1578 keV, ruling out the $9/2$ assignment.

The fits for the angular distribution and the anisotropy for both the 755- and the 758-keV transition are far from optimal, and the ADO values alone are used for tentatively suggested spin values of $11/2$ or $3/2$ for the 1877-keV level and the $2186 + \Delta$ keV level is either $25/2$ or $17/2$. Of the two possible spin values for the $2186 + \Delta$ keV level, the $25/2$ is the more likely one, as the level decays to the $1427 + \Delta$ keV level and not to the $17/2^+$ level at 1427 keV. These transitions and involved levels are shown in Fig. 2.

The 1108-keV transition in $^{210}$Po, between $2^+$ levels at 2290 and 1181 keV, affects the anisotropy and angular distribution analysis of the 1110-keV transition in $^{211}$Po between the 1797-keV and the $11/2^+$, at 687 keV, levels. The ADO value for the 1110-keV $\gamma$-ray transition points to a stretched dipole transition and since the 1797-keV level also decays to the 1427-keV level with a spin value of $17/2^+$, the level in question, shown in Fig. 3, is assigned the spin value of $13/2$.

## IV. DISCUSSION

This section aims to clarify the configurations of certain levels in terms of the shell model. Even though many levels do not have spin and parity assigned to them, it is still possible to deduce configurations from the apparent decay paths and by comparing the levels in $^{211}$Po with its close neighboring nuclei. The main configurations assigned to levels in $^{211}$Po are summarized in Table II. Quantitative comparison between the configuration assignments made in this work will be compared with model calculations in a future publication.

The four first exited levels in $^{210}$Po have the $\pi(h_{9/2})^2$ configuration and are $2^+$ at 1181 keV, $4^+$ at 1427 keV, $6^+$ at 1473 keV, and $8^+$ at 1557 keV [21]. In $^{211}$Po most of the energetically lower levels are expected to originate from the $\pi(h_{9/2})^2_{2^+-6^+} \otimes \nu g_{9/2}$ configurations. Surely enough, the highest spin states of these configurations are found, i.e., the $(2^+ \otimes \nu g_{9/2})_{13/2^+}$ at 1181 keV and the $(4^+ \otimes \nu g_{9/2})_{17/2^+}$ at 1427 keV, and the $1427+\Delta$ keV level is assumed to be the $(6^+ \otimes \nu g_{9/2})_{21/2^+}$ state [9].

TABLE II. Main configurations assigned to levels. Levels marked with an asterisk have not yet been identified or the spin value has not been determined.

| $I^\pi$ | $E_{\text{level}}$(keV) | Configuration |
|---|---|---|
| $9/2^+$ | 0 | $\pi(h_{9/2})^2_{0^+} \otimes \nu g_{9/2}$ |
| $11/2^+$ | 687 | $\pi(h_{9/2})^2_{0^+} \otimes \nu i_{11/2}$ |
| $15/2^-$ | 1064 | $\pi(h_{9/2})^2_{0^+} \otimes \nu j_{15/2}$ |
| $5/2$ | 1584 | $\pi(h_{9/2})^2_{0^+} \otimes \nu d_{5/2}$ |
| $1/2$ | 2033 | $\pi(h_{9/2})^2_{0^+} \otimes \nu s_{1/2}$ |
| $1/2$ | 1578 | $\pi(h_{9/2})^2_{0^+} \otimes \nu(g_{9/2})^2_{0^+}(p_{1/2})^{-1}$ |
| $5/2$ | 2223 | $\pi(h_{9/2})^2_{0^+} \otimes \nu(g_{9/2})^2_{0^+}(f_{5/2})^{-1}$ |
| $5/2^+$ | 1050 | $\pi(h_{9/2})^2_{2^+} \otimes \nu g_{9/2}$ |
| $7/2^+$ | 1122 | $\pi(h_{9/2})^2_{2^+} \otimes \nu g_{9/2}$ |
| $9/2^+$ | 1160 | $\pi(h_{9/2})^2_{2^+} \otimes \nu g_{9/2}$ |
| $11/2^+$ | * | $\pi(h_{9/2})^2_{2^+} \otimes \nu g_{9/2}$ |
| $13/2^+$ | 1181 | $\pi(h_{9/2})^2_{2^+} \otimes \nu g_{9/2}$ |
| $1/2$ | 1385 | $\pi(h_{9/2})^2_{4^+} \otimes \nu g_{9/2}$ |
| $3/2$ | 1443 | $\pi(h_{9/2})^2_{4^+} \otimes \nu g_{9/2}$ |
| $5/2$ | 1614 | $\pi(h_{9/2})^2_{4^+} \otimes \nu g_{9/2}$ |
| $7/2$ | 1437 | $\pi(h_{9/2})^2_{4^+} \otimes \nu g_{9/2}$ |
| $9/2$ | 1407 | $\pi(h_{9/2})^2_{4^+} \otimes \nu g_{9/2}$ |
| $11/2$ | 1409 | $\pi(h_{9/2})^2_{4^+} \otimes \nu g_{9/2}$ |
| $13/2$ | * | $\pi(h_{9/2})^2_{4^+} \otimes \nu g_{9/2}$ |
| $15/2$ | 1459 | $\pi(h_{9/2})^2_{4^+} \otimes \nu g_{9/2}$ |
| $17/2$ | 1427 | $\pi(h_{9/2})^2_{4^+} \otimes \nu g_{9/2}$ |
| $21/2$ | $1427+\Delta$ | $\pi(h_{9/2})^2_{6^+} \otimes \nu g_{9/2}$ |
| $21/2$ | 1541 | $\pi(h_{9/2})^2_{8^+} \otimes \nu g_{9/2}$ |
| $25/2$[a] | 1462 | $\pi(h_{9/2})^2_{8^+} \otimes \nu g_{9/2}$ |
| $27/2$[a] | 1819 | $\pi(h_{9/2})^2_{8^+} \otimes \nu g_{9/2}$ |
| $(7/2)$ | 1726 | $\pi(h_{9/2})^2_{2^+} \otimes \nu i_{11/2}$ |
| $(9/2)$ | 1809 | $\pi(h_{9/2})^2_{2^+} \otimes \nu i_{11/2}$ |
| $11/2$ | 1815 | $\pi(h_{9/2})^2_{2^+} \otimes \nu i_{11/2}$ |
| $13/2$ | 1877 | $\pi(h_{9/2})^2_{2^+} \otimes \nu i_{11/2}$ |
| $15/2$ | 1944 | $\pi(h_{9/2})^2_{2^+} \otimes \nu i_{11/2}$ |
| * | 2253 | $\pi(h_{9/2})^2_{2^+} \otimes \nu j_{15/2}$ |
| $17/2$ | 2314 | $\pi(h_{9/2})^2_{2^+} \otimes \nu j_{15/2}$ |
| $11/2$ | 2352 | $\pi(h_{9/2})^2_{2^+} \otimes \nu j_{15/2}$ |
| $(13/2)$ | 2406 | $\pi(h_{9/2})^2_{2^+} \otimes \nu j_{15/2}$ |
| * | 2448 | $\pi(h_{9/2})^2_{2^+} \otimes \nu j_{15/2}$ |
| $(25/2)$ | $2188+\Delta$ | $\pi(h_{9/2}f_{7/2})_{8^+} \otimes \nu g_{9/2}$ |

[a]Taken from McGoram *et al.* [9]

### A. The $\pi(h_{9/2})^2_{2^+-8^+} \otimes \nu g_{9/2}$ configurations

In Fig. 8, the current assignments of the $\pi(h_{9/2})^2_{2^+-8^+} \otimes \nu g_{9/2}$ configurations are shown compared to the equivalent $\pi(h_{9/2})^2$ multiplets of the $^{210}$Po nucleus. Out of five possible

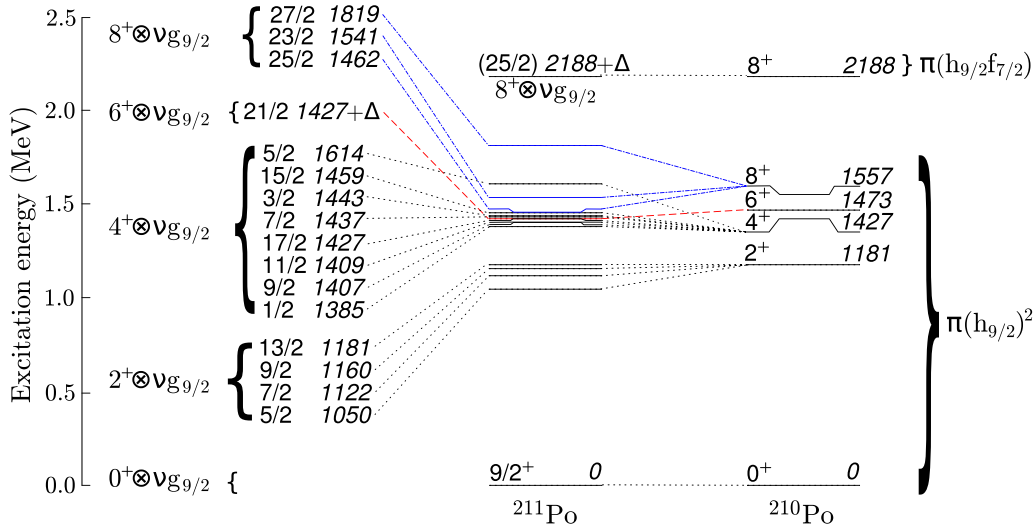


FIG. 8. The $\pi(h_{9/2})^2_{0^+-8^+}$ states and the $\pi(h_{9/2}f_{7/2})_{8^+}$ state in $^{210}$Po are compared to the currently assigned states forming the equivalent $\pi(h_{9/2})^2_{2^+-8^+} \otimes \nu g_{9/2}$ multiplets and the $\pi(h_{9/2}f_{7/2})_{8^+} \otimes \nu g_{9/2}$ state in $^{211}$Po. Note that the states next to the brackets are considered to have positive parity. The $^{210}$Po data is taken from Ref. [21].

levels from the $\pi(h_{9/2})^2_{2^+} \otimes \nu g_{9/2}$ configuration, only four are still identified. These are the $5/2^+$ at 1050 keV, $7/2^+$ at 1122 keV, $9/2^+$ at 1160 keV, and as mentioned earlier the $13/2^+$ at 1181 keV. In the current work, the missing $11/2^+$ level was not found.

Looking at the $^{211}$Bi nucleus, one finds a similar story of only four out of five contenders for the corresponding configuration [22,23]. The elusiveness of the $11/2^+$ state in $^{211}$Po is mentioned in Ref. [8] by Warburton by remarking that the $k = 2$ and 3, i.e., second and third, $11/2$ levels were predicted to have the spectroscopic factor values, $S_n^+$, below that of perception for the $^{210}$Po$(d,p)$ reaction. As the $k = 3$ $11/2$ state was identified in current work with the $^{208}$Pb$(\alpha,\gamma n)$ reaction as the 1409-keV level, one is left to wonder why the $k = 2$ $11/2^+$ is not apparent.

The $\pi(h_{9/2})^2_{4^+} \otimes \nu g_{9/2}$ configuration should have nine states between spin values of $17/2$ and $1/2$. The following eight levels seem to fit as states belonging to the $\pi(h_{9/2})^2_{4^+} \otimes \nu g_{9/2}$ configuration: 1427 $17/2^+$, 1459 $15/2^+$, 1409 $11/2^+$, 1407 $9/2^+$, 1437 $7/2^+$, 1614 $5/2^+$, 1443 $3/2^+$, and 1385 $1/2^+$ keV. The $13/2^+$ level is still missing from the complete multiplet and probably resides within 1385- to 1427-keV energy region.

The $17/2^+$ level at 1427 keV will also be brought up to discussion, in the mixed level configurations, Subsec. IV H, due to its decay to the $15/2^-$ level at 1064 keV. The decay between these two levels could be seen as the transition between $\pi(h_{9/2})^2_{4^+} \otimes \nu g_{9/2}$ and $\pi(h_{9/2})^2_{0^+} \otimes \nu j_{15/2}$. As will be discussed, this unlikely transition is made possible due to octopole mixing of the latter state.

Assigning levels to the $\pi(h_{9/2})^2_{6^+} \otimes \nu g_{9/2}$ configuration is harder compared to previous configurations with current data and the lack of theoretical coverage of said configuration. In this configuration, 10 states are expected with spin values ranging from $21/2$ down to $3/2$, and with the $21/2$ level locked as the 1427+Δ keV level, the remaining 9 have to depend on future endeavors.

The $\pi(h_{9/2})^2_{8^+} \otimes \nu g_{9/2}$ configuration was not part of this study as these levels are hard to reach with currently used reactions and energy. Still, a few words can be said about it. The $25/2^+$ isomer at 1462 keV is from the $\pi(h_{9/2})^2_{8^+} \otimes \nu g_{9/2}$ configuration, which yields 13 states with spin values ranging from $25/2$ to $7/2$. The $27/2^+$ at 1820 keV is the only other level previously assigned to this configuration [9]. With current data, another level belonging to this multiplet is most likely the $21/2$ level at 1541 keV.

### B. The $\pi(h_{9/2})^2_{2^+-4^+} \otimes \nu i_{11/2}$ configurations

Besides the levels mentioned in Fant *et al.* [7], a further three levels are added to the list of possible candidates of the $\pi(h_{9/2})^2_{2^+} \otimes \nu i_{11/2}$ configuration. The list would then be as follows: 1678, 1715, 1726, 1797, 1809, 1815, 1877, and 1944 keV. With some degree of confidence, the levels 1679 and 1797 keV can ruled out by examining other decay routes these levels take. Both mentioned levels, for example, also have transitions to $\pi(h_{9/2})^2_{4+} \otimes \nu g_{9/2}$ configuration levels, therefore making their inclusion in the $\pi(h_{9/2})^2_{2^+} \otimes \nu i_{11/2}$ configuration unlikely. Some of the candidate levels have only the dipole or quadrupole nature of their decay transitions known. Considering that spin values of the $2^+ \otimes \nu g_{9/2}$ levels start with the $5/2^+$ to the $13/2^+$ in ascending order, one would expect the situation to be the same in the $2^+ \otimes \nu i_{11/2}$ case. With this in mind, the following levels, with corresponding spins 1726 (7/2), 1809 (9/2) 1815 11/2, 1877 (13/2), and 1944 (15/2), are suggested as the $2^+ \otimes \nu i_{11/2}$ multiplet and are shown in Fig. 3.

The $\pi(h_{9/2})^2_{4^+} \otimes \nu i_{11/2}$ configuration should give us 9 states with spin values ranging from $19/2$ to $3/2$. Based upon the $\gamma$-ray decay and level scheme, the following levels of 2042, 2144, 2150, 2189, and 2313 keV, shown in Fig. 3 are considered as

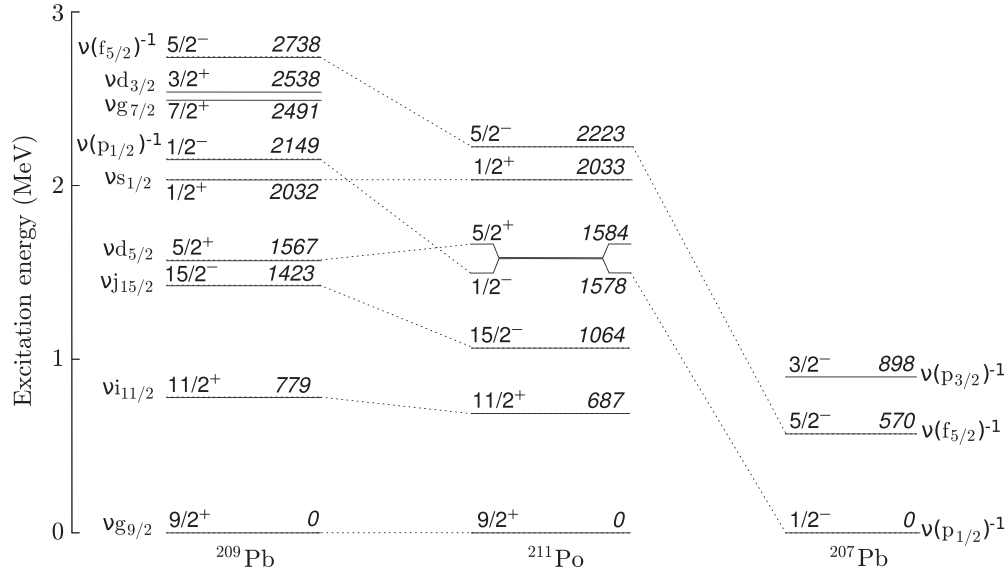


FIG. 9. Comparison of single-particle states and hole states in $^{207}$Pb, $^{209}$Pb, and $^{211}$Po. The reference data for $^{207}$Pb are taken from Ref. [20], $^{209}$Pb data are taken from Refs. [24–26], and $^{211}$Po data are taken from Refs. [7,9] and current work.

originating from this configuration and are most likely in the middle of the possible multiplet spin range. The higher and lower end spin levels from this multiplet are expected to decay along other paths as the spin difference to the $11/2^+$ level at 687 keV will be too large.

### C. The $\pi(h_{9/2})^2_{2^+-4^+} \otimes \nu j_{15/2}$ configurations

The levels at 2253, 2314 (17/2), 2352 (11/2), 2406 (13/2), and 2448 keV, shown in Fig. 3, are considered to be candidates for the $\pi(h_{9/2})^2_{2^+} \otimes \nu j_{15/2}$ configuration levels. The 2448-keV level is somewhat problematic as the spin for this level is measured to be either 13/2 or 17/2, and these spin values are already tentatively assigned to the 2406 and 2314-keV levels respectively. This means that one of the above mentioned levels does not belong the $2^+ \otimes \nu j_{15/2}$ multiplet. In the search for other candidate levels, it is prudent to remember that 48% of the $15/2^-$ level at 1064 keV is $3^- \otimes \nu g_{9/2}$ [4]. With this mixing in mind, the levels from the $2^+ \otimes \nu j_{15/2}$ multiplet could also include admixture of the form $2^+ \otimes (3^- \otimes \nu g_{9/2})$ and decay to the $4^+ \otimes \nu g_{9/2}$ levels would be possible. There are other levels in the relevant energy region; e.g., the mean value of the $2^+$ in $^{210}$Po at 1181 keV added to the energy of $j_{15/2}$ in $^{211}$Po at 1064 keV yields an energy of 2245 keV, but without explicit measured spin and parity it is hard to determine which final level should be included.

With higher energy, the 2622- and 2701-keV levels are then considered to belong from the $\pi(h_{9/2})^2_{4^+} \otimes \nu j_{15/2}$ configuration. The 2448-keV level mentioned earlier in the discussion might actually originate in this multiplet. As in the case of the $\pi(h_{9/2})^2_{4^+} \otimes \nu i_{11/2}$ configuration levels, these levels are probably from the middle of the configuration spin range.

### D. Single-neutron particle states of $\nu d_{5/2}$ and $\nu s_{1/2}$

The single-neutron states $\nu d_{5/2}$ and $\nu s_{1/2}$ in $^{209}$Pb reside at 1567 and 2032 keV, respectively [24–26]. In the current work, the assigned levels for the corresponding single-particle states in $^{211}$Po are the (5/2) level at 1584 keV and the 1/2 level at 2033 keV, shown in the level scheme presented in Fig. 4. Also, a comparison between the single-particle states in $^{209}$Pb and the currently assigned single-particle states $^{211}$Po are shown in Fig. 9. The single-neutron states of $\nu g_{7/2}$ and $\nu d_{3/2}$ are found at the energies of 2449 and 2547 keV respectively in $^{209}$Pb [24]. With current data, there are no levels with the right energy and spin for a corresponding $\nu g_{7/2}$ state in $^{211}$Po. The level at 2547 keV in $^{211}$Po would be the perfect candidate for the $\nu d_{3/2}$ state energywise, but without a measured spin value for this level it is difficult to asses which configuration it belongs to. So, out of the three states with predicted neutron halos in $^{211}$Po [12], two, i.e., the $\nu d_{5/2}$ and $\nu s_{1/2}$ states, are now identified.

The $\pi(h_{9/2})^2_{2^+} \otimes \nu d_{5/2}$ configuration, with spins from $9/2^+$ to $5/2^+$, would probably end being around an energy of 2765 keV, i.e., the $2^+$ in $^{210}$Po at 1181 keV added to the energy of the $d_{5/2}$ in $^{211}$Po at 1584 keV.

### E. The $\pi(h_{9/2})^2_{0^+} \otimes \nu(g_{9/2})^2_{0^+}(n)^{-1}$ configurations

The 1578-keV level was proposed in Ref. [7] to be the first neutron hole $\nu p^{-1}_{1/2}$ level. The spin and parity for the 1578-keV level was evaluated to be $1/2^-$ in Ref. [7] and its measured half-life of 3.5 ns correlates well with the half-life of 3.96 ns [27] of the corresponding neutron hole, $\nu p^{-1}_{1/2}$, at 2149 keV in $^{209}$Pb [24]. The $\gamma$-ray transition of 645 keV, between 2224- and 1578-keV levels in $^{211}$Po, shows quadrupole properties supporting the idea that it is the next neutron hole $\nu f^{-1}_{5/2}$. The neutron hole levels in $^{211}$Po, i.e., 1578 and 2224 keV, are shown in the level scheme in Fig. 4. In Fig. 9, these two states are compared to the neutron holes in $^{207}$Pb and $^{209}$Pb.

As can be seen, the neutron holes in $^{211}$Po are similarly spaced as their corresponding neutron holes in $^{207}$Pb [20] and $^{209}$Pb [24]. Although when comparing $^{211}$Po with $^{209}$Pb, there

is a rather large energy shift between the corresponding neutron levels. The $\nu p^{-1}_{1/2}$ and $\nu f^{-1}_{5/2}$ levels in $^{211}$Po are less bound by 500 keV then those in $^{209}$Pb [24]. Considering that the corresponding neutron single-particle states in $^{211}$Po and $^{209}$Pb are very close to the same, this energy shift in the neutron hole states seem peculiar and the reason for this energy shift is currently unknown. With this in mind though, one would expect the $\nu i^{-1}_{13/2}$ neutron hole state in $^{211}$Po to be around an excitation energy of about 3100 keV, i.e., still beyond the energy reach of current work.

What possible configurations can the $\nu p^{-1}_{1/2}$ state in $^{211}$Po decay to? Since the $\nu p^{-1}_{1/2}$ neutron hole at 1578 keV decays to the 1385-keV level, which is assigned to the $\pi(h_{9/2})^2_{4^+} \otimes \nu g_{9/2}$ configuration, see Subsec. IV A, the $\pi(h_{9/2})^2$ protons would have to undergo a change from $4^+$ to $0^+$, and the neutron would have to go back from the $\nu g_{9/2}$ state to $\nu p_{1/2}$. The spin change between $\nu g_{9/2}$ and $\nu p_{1/2}$ is already 4, making a $\gamma$-ray transition unlikely. For this transition to be possible, either or both levels need mixing of some sort in their configurations. The mixed level configuration of neutron hole levels could, perhaps, explain the above-mentioned energy shift. What possible states are there then that would mix with the $\nu p^{-1}_{1/2}$ state?

### F. The $\pi(h_{9/2}f_{7/2})_{8^+} \otimes \nu g_{9/2}$ configuration

The lowest level from the $\pi(h_{9/2}f_{7/2})$ configuration in $^{210}$Po is the $8^+$ level at 2188 keV [21]. Now a corresponding level coupled to the $\nu g_{9/2}$ in $^{211}$Po nucleus should yield a $25/2^+$ level at a similar energy. The spin for the $2186+\Delta$ keV level is tentatively assigned the spin value of 25/2 and fits nicely in as the level in question. Both levels are shown in the comparison of configurations between $^{210}$Po and $^{211}$Po in Fig. 8.

### G. The $3^- \otimes \nu g_{9/2}$ and other collective vibrations

As mentioned in Faestermann *et al.* [4], the measurements seem to conclude that the 1064-keV state is 52% $\nu j_{15/2}$ and 48% $3^- \otimes \nu g_{9/2}$. This leads to the question of where the rest of the above-mentioned strengths are in $^{211}$Po. The corresponding $15/2^-$ level at 1423 keV in $^{209}$Pb is cited as containing about 30% of the $\nu j_{15/2}$ while the $(15/2^-)$ level at 3047 keV contains the majority of the $3^- \otimes \nu g_{9/2}$ configuration [25]. The 3047-keV level de-excites to the 1423-keV level with a 1624-keV $\gamma$ ray [25]. A corresponding 3047-keV level in $^{211}$Po lies outside the energy region of current study and is not recorded elsewhere either. Are there other states with the collective vibrations in their configuration within current experimental regions of energy? One possibility is to have a single neutron in the $\nu j_{15/2}$ orbital coupled to a higher multipole core, i.e., $|25/2^+\rangle = |5^- \otimes j_{15/2}\rangle$. If that is the case, then one might have the exotic possibility, although unlikely, of an allowed and electrically fast $E5$ component to the $15/2^-$ 1064-keV state. To characterize this transition, a pulsed measurement is needed.

### H. Mixed level configurations

There are transitions between certain levels that are slightly problematic from the perspective of pure level configurations, for example, as already mentioned in Subsec. IV E, the transition between the $1/2^-$ level at 1578 keV and level $1/2^+$ at 1385 keV. The pure state transition would be between the $(\pi(h_{9/2})^2_{0^+} \otimes \nu p^{-1}_{1/2})_{1/2^-}$ and the $(\pi(h_{9/2})^2_{4^+} \otimes \nu g_{9/2})_{1/2^+}$ state configurations.

There are some levels with mixed configurations that are perhaps easier to understand. These levels, connected via $\gamma$-ray decay, are the $17/2^+$ level at 1427 keV and the $15/2^-$ level at 1064 keV, the $9/2^+$ at 1160 keV and the $11/2^+$ at 687 keV and finally the $13/2^+$ at 1181 keV and the $11/2^+$ at 687 keV. The $17/2^+$ level at 1427 keV decays with a 363-keV $\gamma$ ray and the $9/2^+$ at 1160 keV and $13/2^+$ at 1181 keV decay with 474 and 494 keV transitions, respectively.

Considered from an unmixed perspective, the 363-keV transition would be between the configurations $(\pi(h_{9/2})^2_{4^+} \otimes \nu g_{9/2})_{17/2^+}$ and $(\pi(h_{9/2})^2_{0^+} \otimes \nu j_{15/2})_{15/2^-}$, making the transition highly unlikely. As the 1064-keV level is partly of the $3^- \otimes \nu g_{9/2}$ configuration [4], the transition between these two levels is more likely as a dipole transition between $4^+$ and the $3^-$ octupole configurations while retaining the $\nu g_{9/2}$ unchanged. Both the $9/2^+$ at 1160 keV and $13/2^+$ at 1181-keV levels are from the $(\pi(h_{9/2})^2_{2^+} \otimes \nu g_{9/2})$ configurations and the $11/2^+$ at the 687-keV level is of the form $(\pi(h_{9/2})^2_{0^+} \otimes \nu i_{11/2})$. In this transition on the proton side, the $2^+$ de-excites to a $0^+$ and excites the neutron from $g_{9/2}$ to $i_{11/2}$. Would a mixed configuration in either involved levels make the transition less arduous?

Other levels that need mixing of some sort between them are the (5/2) level at 1584 keV and the $5/2^+$ level at 1050 keV connected through the 534-keV transition and the 1/2 level at 2033 keV with decay to both the $5/2^+$ level at 1050 keV and $1/2^-$ level at 1578 keV with the 982- and 455-keV transitions, respectively. The configurations for the levels involved in the transition the (5/2) level at 1584 keV to $5/2^+$ level at 1050 keV are considered to be $(\pi(h_{9/2})^2_{0^+} \otimes \nu d_{5/2})_{5/2^+}$ and $(\pi(h_{9/2})^2_{2^+} \otimes \nu g_{9/2})_{5/2^+}$. With these configurations, the transition between them de-excites the neutron from the $d_{5/2}$ to the ground state and excites the proton side from $0^+$ to $2^+$. With both levels having the same spin (and assumed parity), it is not without reason to expect either, or both, levels to contain fractions of the other levels configuration strengths.

The 1/2 level at 2033 keV with the $(\pi(h_{9/2})^2_{0^+} \otimes \nu s_{1/2})_{1/2^+}$ configuration decays to both the $(\pi(h_{9/2})^2_{2^+} \otimes \nu g_{9/2})_{5/2^+}$ and the $(\pi(h_{9/2})^2_{0^+} \otimes \nu s^{-1}_{1/2})_{1/2^-}$ configurations. From the above discussion about the levels involved in the 534-keV $\gamma$-ray transition, it was mentioned that the $5/2^+$ level at 1050 keV might contain configuration strengths from the $d_{5/2}$ configuration. If this is the case, then the 455-keV transition could be seen as de-exciting the neutron from $\nu s_{1/2}$ to $\nu d_{5/2}$. In that note, it is interesting that there is no apparent transition between the 1/2 and (5/2) levels at 2033 and 1584 keV, respectively.

The $1/2^-$ level at 1578 keV was also mentioned before in the discussion of the levels involved in the 193-keV transition and a mixing of the initial and/or final levels would also help the transition between these two states.

## V. SUMMARY AND OUTLOOK

The fusion-evaporation reaction $^{208}$Pb$(\alpha,n)^{211}$Po, with 23-MeV $\alpha$ particles, has been studied with in-beam $\gamma$-ray

spectroscopy at JYFL to characterize the low- and medium-spin structure of $^{211}$Po. All in all, 158 $\gamma$-transitions originating from $^{211}$Po were detected, and 76 of these are seen for the first time. The low- and medium-spin level scheme of $^{211}$Po, developed in present work, was improved substantially compared to Refs. [7,9]. From a structural point of view, the configurations $\pi(h_{9/2})^2_{2^+-4^+} \otimes \nu g_{9/2}$, $\pi(h_{9/2})^2_{8^+} \otimes \nu g_{9/2}$, $\pi(h_{9/2})^2_{2^+-4^+} \otimes \nu i_{11/2}$ $\pi(h_{9/2})^2_{2^+-4^+} \otimes \nu j_{15/2}$ and $\pi(h_{9/2}f_{7/2})_{8^+} \otimes \nu g_{9/2}$ were extended with new levels assigned to them. The single-particle neutron states $\nu d_{5/2}$ and $\nu s_{1/2}$ were identified as well as the neutron hole state of $\nu(g_{9/2})^2_{0^+}(f_{5/2})^{-1}$. Also the need of mixed levels for some transitions to work between certain configurations was discussed. Comprehensive calculations are currently under way to explore the theoretical aspects of the $^{211}$Po nucleus more quantitatively; these results will be presented in an upcoming article.

## ACKNOWLEDGMENTS

The authors would like to thank the the UK/France detector Loan Pool and GAMMAPOOL European Spectroscopy Resource for the loan of detectors for the JUROGAM array. We would also like to thank the JYFL accelerator staff. J.M.K. acknowledges support from the Swedish Cultural Foundation in Finland. J.M.K. also would like to thank D. C. Radford for kindly providing valuable insight in the usage of RADWARE packages.

[1] L. Coraggio, A. Covello, A. Gargano, N. Itaco, and T. Kuo, Prog. Part. Nucl. Phys. **62**, 135 (2009).
[2] I. Talmi, Adv. Nucl. Phys. **27**, 143 (2003).
[3] N. Auerbach and I. Talmi, Phys. Lett. **10**, 297 (1964).
[4] T. Faestermann, F. Feilitzsch, K. E. G. Löbner, C. Signorini, T. Yamazaki, C. V. K. Bada, and D. B. Fossan, J. Phys. Soc. Jpn. Suppl. **34**, 287 (1973).
[5] T. S. Bhatia, T. R. Canada, P. D. Barnes, R. A. Eisenstein, and C. Ellegaard, Nucl. Phys. A **314**, 101 (1979).
[6] B. Silvestre-Brac and J. P. Boisson, Phys. Rev. C **24**, 717 (1981).
[7] B. Fant, T. Lönnroth, and V. Rahkonen, Nucl. Phys. A **355**, 171 (1981).
[8] E. K. Warburton, Phys. Rev. C **44**, 1500 (1991).
[9] T. R. McGoram, G. D. Dracoulis, A. P. Byrne, A. R. Poletti, and S. Bayer, Nucl. Phys. A **637**, 469 (1998).
[10] B. Fornal, R. Broda, W. Królas, T. Pawlat, J. Wrzesiński, P. J. Daly, P. Bhattacharyya, Z. W. Grabowski, C. T. Zhang, D. Bazzacco *et al.*, Eur. Phys. J. A **1**, 355 (1998).
[11] B. Fornal, R. Broda, W. Królas, T. Pawlat, J. Wrzesiński, P. J. Daly, P. Bhattacharyya, Z. G. C. T. Zhang, D. Bazzacco, S. Lunardi *et al.*, Acta Phys. Pol. B **30**, 1219 (1999).
[12] Q. Sun and J.-Y. Guo, Chin. Phys. C **33**, 130 (2009).
[13] I. H. Lazarus, D. E. Appelbe, P. J. Coleman-Smith, J. Cresswell, S. J. Freeman, R. D. Herzberg, I. Hibbert, D. T. Joss, S. C. Letts, R. D. Page *et al.*, IEEE Trans. Nucl. Sci. **48**, 567 (2001).
[14] P. Rahkila, Nucl. Instr. Meth. Phys. Res. A **595**, 637 (2008).
[15] D. C. Radford, Nucl. Instr. Meth. Phys. Res. A **361**, 297 (1995).
[16] D. C. Radford, Nucl. Instr. Meth. Phys. Res. A **361**, 306 (1995).
[17] T. Yamazaki, Nucl. Data Sheets. Section A **3**, 1 (1967).
[18] M. Piiparinen, A. Ataç, J. Blomqvist, G. Hagemann, B. Herskind, R. Julin, S. Juutinen, A. Lampinen, J. Nyberg, G. Sletten *et al.*, Nucl. Phys. A **605**, 191 (1996).
[19] A. R. Barnett and J. S. Lilley, Phys. Rev. C **9**, 2010 (1974).
[20] M. Kadi, P. E. Garrett, M. Yeh, S. W. Yates, T. Belgya, A. M. Oros-Peusquens, and K. Heyde, Phys. Rev. C **61**, 034307 (2000).
[21] L. G. Mann, K. H. Maier, A. Aprahamian, J. A. Becker, D. J. Decman, E. A. Henry, R. A. Meyer, N. Roy, W. Stöffl, and G. L. Struble, Phys. Rev. C **38**, 74 (1988).
[22] E. Flynn, D. Burke, J. Sherman, and J. Sunier, Nucl. Phys. A **263**, 365 (1976).
[23] E. Browne, Nucl. Data Sheets **103**, 183 (2004).
[24] G. Igo, E. R. Flynn, B. J. Dropesky, and P. D. Barnes, Phys. Rev. C **3**, 349 (1971).
[25] M. Rejmund, K. H. Maier, R. Broda, B. Fornal, M. Lach, J. Wrzesiński, J. Blomqvist, A. Gadea, J. Gerl, M. Górska *et al.*, Eur. Phys. J. A **1**, 261 (1998).
[26] M. Martin, Nucl. Data Sheets **63**, 723 (1991).
[27] V. M. Datar, C. V. K. Baba, S. N. Acharya, S. A. Chitambar, H. C. Jain, S. K. Bhattacherjee, and C. S. Warke, Phys. Rev. C **22**, 1787 (1980).